UNIVERSIDAD DE CONCEPCIÓN
FACULTAD DE CIENCIAS FÍSICAS Y MATEMÁTICAS

Weakly Non-Linear Interaction Between Electromagnetic and Electrostatic Spectra in a Solar Wind-Type Plasma

by

B.Sc. Martín Andrés Quijada Benavente

Thesis submitted to the Faculty of Physical Sciences and Mathematics of the University of Concepción in partial fulfillment of the requirements for the degree of Master in Sciences with Major in Physics

June 2025
Concepción, Chile

Advisor: Dr. Roberto Navarro Maldonado

... Todo ocurre en el triángulo de las Bermudas.
Ojos para ver, oreja para escuchar y mente para interpretar.
— Fernando Cifuentes Cáceres

Acknowledgements

Si bien la mayoría del presente documento es presentado en inglés para su lectura académica, quiero permitirme esta sección en mi lengua materna. A diferencia de Borges, no creo que la lengua anglosajona pueda hacerle justicia al peso y significación que deseo otorgar a las palabras que aquí escritas, hago hacia quienes agradezco desde lo más profundo en la lengua de Cervantes.

En primer lugar, agradecer a mis padres, que sin muchas veces entender lo que hago y el por qué de las decisiones que tomo –como estudiar esta carrera–, me han apoyado y dado las oportunidades para estar donde estoy hoy. Sin duda que eso me ha llevado lejos y este es uno de los frutos. A mis hermanas, María Fernanda y Matilda por su cariño, que sin ello no hubiese sobrevivido más de un día. A mis abuelos y abuelas; Rubén, Norma, Susana y Rodolfo, siempre atentos a mi devenir, curiosos por mi siguiente paso. Me acompañarán siempre.

A mi tío y primer profesor, Andrés Castro, que en donde sea que esté, marca el inicio de todo esto y más. Je t'embrasse, mon oncle.

A las futuras doctoras, María José, Monserrat y Arelly; mis amigas de la universidad, y ahora también de la vida. Expresarles mi mayor gratitud y admiración; además de desearles el mayor de los éxitos en los rumbos que ya han emprendido. La carga se hizo más ligera con ustedes en el andar.

A Danilo Rivera, en quien encontré una noble amistad y un optimismo contagioso, y por enseñarme `.hdf5`; a la camaradería de Nelson Villalba, a Hugo Carril y Jorge Gidi, a quienes miro y he compartido como hermanos mayores.

A mis compañeros: Alejandro Saavedra, Lilianne Tapia, Cielo Ramírez, Benjamín Hernández, Vicente Cárdenas, Pedro Contreras, Constanza Rivas, Adheris Contreras, Tomás Troncoso, Tomás Moraga y Lucas Sanhueza. Con quienes he compartido más de un café, una conferencia, una conversación para subir la moral, un viaje, una visita al laboratorio, un almuerzo, un trasnoche. Gracias por el mutuo apoyo y aguante. Mis mejores deseos a cada uno de ustedes.

A mis amigos de hace ya mucho: Felipe, Joaquín, Matías, Gaspar, Javier, Agustín. Gracias por tanto. Ustedes saben lo importante que han sido todos estos años. Y a sus familias, por acogerme en sus hogares y siempre hacerme sentir como uno más. Estoy en deuda.

Al cuerpo académico: al Dr. Roberto Navarro quien me recibió, apoyó, confió en mis capacidades y me enseñó a forjar las competencias necesarias para llevar a cabo esta investigación. A Pablo Moya, por la motivación y ser el pivote clave para el artículo que nace de esta tesis de magíster. A Julio Oliva, que yo sin ser gravitólogo, he recibido su aliento y energía en mi pasar por la universidad, además de ser un ejemplo de dedicación y entrega –Siga manteniéndose fuerte, profesor. A Pablo Solano y Hernán Astudillo, de quienes tomo sus invaluables experiencias compartidas en una que otra conversación de pasillo. Gracias por sus palabras.

A mis profesores del colegio: Sergio Neira, quien vió más entusiasmo que talento y me invitó a adentrarme en esta aventura de la física sin saber en qué depararía; a Magdiel Fuentealba, por aquella tarde de viernes donde me enseñó a escudriñar en el mundo del átomo y que ha repercutido hasta el día de hoy; y a Pablo Parada, por su calidez, nunca perder su capacidad de asombro y además de poder transmitirla. A ellos, cuya calidad humana permeó más allá de la enseñanza de la ciencia y las salas de clases.

Por último, agradezco al programa de Magíster en Ciencias con mención en Física del Departamento de Física de la Universidad de Concepción, que mediante la beca de articulación, permitió seguir desarrollándome como profesional y ahorrando preocupaciones financieras a mi familia.

No sólo no hubiéramos sido nada sin ustedes, sino con toda la gente que estuvo a nuestro alrededor desde el comienzo. Algunos siguen hasta hoy. . .

Resumen

En la teoría cinética lineal, los modos de onda electromagnéticos transversales y electrostáticos que se propagan a lo largo de un campo magnético de fondo $\boldsymbol{B}_0$ se consideran desacoplados y se ha estudiado su evolución de forma independiente. No obstante, en plasmas espaciales y astrofísicos reales, las interacciones resonantes entre ondas y partículas introducen no linealidades que rompen esta separación idealizada. Estudiamos la evolución cuasilineal acoplada de ondas Alfvén-ciclotrón (ACWs) y ondas ion-acústicas (IAWs) en un plasma de protones sin colisiones con distribución bi-Maxwelliana. Es de especial interés la razón de temperaturas entre electrones y protones ($10 \leq T_e/T_p \leq 50$) en cómo facilita la influencia indirecta entre estos modos de onda, además de estar en presencia de fluctuaciones del campo eléctrico constantes e independientes del campo magnético de fondo $\boldsymbol{B}_0$. Los resultados muestran que incluso una actividad moderada de ondas ion-acústicas puede acelerar el calentamiento perpendicular de los protones y favorecer la aparición temprana de inestabilidades electromagnéticas ciclotrónicas (EMIC). Este mecanismo representa una vía plausible y eficiente para la energización de protones en plasmas espaciales, con implicancias directas para el viento solar y la magnetósfera, donde tales condiciones son comúnmente observadas. Nuestros resultados contribuyen a ampliar y dar una mayor comprensión de las interacciones entre múltiples modos de onda y los procesos de transferencia de energía en entornos de plasma sin colisiones.

Keywords – Ondas de Alfvén, Ondas Ion-Acústicas, Amortiguamiento de Landau, Calentamiento del plasma, Teoría Cuasilineal, Plasmas espaciales.

Abstract

In linear kinetic theory, transverse electromagnetic and electrostatic plasma wave modes propagating along a background magnetic field $\boldsymbol{B}_0$ are treated as decoupled and evolve independently. However, in realistic space and astrophysical plasmas, resonant wave–particle interactions introduce nonlinearities that break this idealized separation. This thesis investigates the coupled quasilinear evolution of Alfvén-cyclotron waves (ACWs) and ion-acoustic waves (IAWs) in a collisionless, bi-Maxwellian proton plasma. Emphasis is placed on how the electron-to-proton temperature ratio ($10 \leq T_e/T_p \leq 50$) facilitates indirect coupling between these wave modes, particularly when constant electric field fluctuations—independent of the background magnetic field $\boldsymbol{B}_0$—are present. The results demonstrate that even modest levels of ion-acoustic activity can significantly enhance perpendicular proton heating and promote earlier onset of electromagnetic ion cyclotron (EMIC) instabilities. This mechanism offers a plausible and efficient pathway for proton energization in space plasmas, with direct implications for the solar wind and planetary magnetospheres, where such conditions are commonly observed. The findings contribute to a deeper understanding of multi-mode interactions and energy transfer processes in collisionless plasma environments.

Keywords – Alfvén waves, Ion-Acoustic waves, Landau Damping, Plasma heating, Quasilinear theory, Space Plasmas.

Contents

List of Figures

Introduction

The *solar wind* refers to the continuous stream of magnetized, charged particles that flows outward from the solar corona into interplanetary space. Composed primarily of protons and electrons, it also contains heavier ions such as alpha particles, iron and oxygen nuclei. In this environment, the mean free path between particle collisions is comparable to the characteristic dimensions of the system, meaning that binary collisions are scarce. As a consequence, the solar wind can be regarded as a *collisionless* plasma, and its behavior may be best described using kinetic theory, specifically the Vlasov-Maxwell formalism to model its dynamics, self-consistent electromagnetic fields and the external ones.

This plasma exhibits inherent nonlinearity and multiscale dynamics, giving rise to non-thermal features such as temperature anisotropies, heat fluxes, differential streaming between species or double beams, and high-energy tails in the velocity distribution. Early space missions designed to study solar activity, such as the *Pioneer* program and the *Helios* spacecraft, measured velocity distribution functions (VDFs) that significantly deviated from the predictions of thermodynamic equilibrium. These observations suggest the existence of excitation mechanisms for micro-instabilities and electromagnetic fluctuations, potentially associated with any of the plasma species, either individually or collectively. Over time, it has been established that if an instability develops, it tends to saturate due to energy constraints, such that the resulting temperature anisotropy remains bounded. These bounds are primarily set by the thresholds of well-known instabilities, including the firehose, mirror, and electromagnetic ion cyclotron (EMIC) instabilities, among the most extensively studied in space plasmas.

The spectral (Fourier–Laplace) analysis enabled by the kinetic theory framework allows the identification of propagating modes for a given physical configuration. One of the main objectives of this thesis was to investigate the interaction between two such modes which, at first glance, appear decoupled within the scope of linear theory. This analysis was carried out under the assumption of parallel propagation in a uniform background magnetic field and developed analytically through quasilinear moment theory [1, 2]. A parametric numerical study was then conducted to examine the macroscopic properties of the plasma and to understand how one mode perturbs the adiabatic evolution of the other. Here we consider the Alfvén–Cyclotron Wave (ACW), which is well documented in the literature for its role in generating magnetic fluctuations [3]; on the other hand, we focus on the Ion-Acoustic Wave (IAW), whose coupling in this context—associated with electric field fluctuations—constitutes the novel contribution of this work.

Electrostatic fluctuations associated with ion-acoustic waves have been extensively investigated and reported [4, 5, 6, 7], not only in collisionless plasmas but also in laboratory conditions after the first Langmuir probes [8, 9]. In space environments, these spectra waves were detected in the kiloHertz range propagating parallel to the ambient magnetic field and firstly reported by D. Gurnett [4, 10], despite that they are subject to strong Landau damping; according to linear Vlasov theory and it has been demonstrated that, as they dissipate, they simultaneously transfer energy to the plasma in the kinetic regime. Nevertheless, these electrostatic signatures cannot be simply interpreted as IAW in typical solar-wind conditions of temperature ratio T_e/T_p [11]. Alternative interpretations based on simulations [12, 13, 14] and observational analyses [15, 16] have been developed to address persistent discrepancies and improve the understanding of this wave spectrum. The evidence in the last decade linking the Alfvénic scales with the electrostatic ones has been promising [14, 17] and also contrasted by several numerical methods: PIC, hybrid Vlasov-Maxwell [18], Vlasov-Yukawa [19]. They reveal a cross-scale energy transfer mechanism despite the large separation in spatial and temporal scales.

The following sections present the theoretical framework, numerical methodology, and a discussion of the main results. We conclude with a summary of the key contributions of this study to the understanding of multi-mode kinetic interactions in collisionless plasmas.

Chapter 1

Linear and Quasilinear Theory

In this first chapter, we present and develop the calculations required within the framework of linear kinetic theory to describe wave propagation modes in a collisionless plasma—i.e., with solar wind-type characteristics—assuming parallel propagation with respect to a uniform background magnetic field. In addition, we present the theoretical framework underlying the kinetic formalism and specify the equilibrium conditions assumed in the analysis.

Subsequently, we extend the analysis to second-order perturbative calculations within the same kinetic framework, leading to the formulation of *quasilinear moment theory*, which allows us to derive the key governing equations for a bi-Maxwellian velocity distribution function.

1.1 Vlasov-Maxwell formalism

A kinetic-statistical description of an ensembles of charged particles q_μ (electrons, protons, alpha particles, etc.) under the influence of a constant background magnetic field $\boldsymbol{B_0}$ is needed due the lack of a fluid description of giving a satisfactory response to resonance phenomena such as cyclotron resonance or Landau damping because of the short-range interactions considered in this theory.
We seek to characterize a system compound of many N particles as possible to have long-range interactions in a volume V, so that exhibits collective behavior. Yet low enough in an average density $n \equiv N/V$, so that the force due to a near-neighbour particle is much less than the Coulomb force exerted by the many distant particles [11], i.e. $n \lesssim 1$. What is more, it has to be *quasineutral*, that is to say, the sum of $q_\mu n \simeq 0$ but not null that the interesting electromagnetic forces vanish. For these reasons, the Vlasov [20] equation is employed for a $\mu-$species plasma, providing a more accurate phenomenology by capturing the collisionless dynamics and wave-particle interactions essential to the study of this work in the space plasmas context.

This yields,

$$\left[\frac{\partial}{\partial t} + \boldsymbol{v} \cdot \frac{\partial}{\partial \boldsymbol{x}} + \frac{q_\mu}{m_\mu}\left(\boldsymbol{E}(\boldsymbol{x},t) + \frac{\boldsymbol{v} \times \boldsymbol{B}(\boldsymbol{x},t)}{c}\right) \cdot \frac{\partial}{\partial \boldsymbol{v}}\right] f_\mu(\boldsymbol{x},\boldsymbol{v},t) = 0. \tag{1.1.1}$$

It is a conservative equation that describes the temporal and spatial changes of a collisionless distribution of particles $f_\mu(\boldsymbol{x},\boldsymbol{v},t)$ under the influence of the Lorentz force. Consequently, it becomes essential and mandatory to use Maxwell equations that grant the sources of this physical scenario, scaling quickly from statistical mechanics to electrodynamics due the presence of both external electric and magnetic fields involved in addition to those that emerges from the plasma itself, resulting a rich and complex system dynamics.

Maxwell equations (in CGS units system) yield,

$$\nabla \cdot \boldsymbol{E} = 4\pi\rho, \tag{1.1.2}$$

$$\nabla \cdot \boldsymbol{B} = 0, \tag{1.1.3}$$

$$\nabla \times \boldsymbol{E} = -\frac{1}{c}\frac{\partial \boldsymbol{B}}{\partial t}, \tag{1.1.4}$$

$$\nabla \times \boldsymbol{B} = \frac{1}{c}\frac{\partial \boldsymbol{E}}{\partial t} + \frac{4\pi}{c}\boldsymbol{J}. \tag{1.1.5}$$

In this study we will refer to the relevant (Maxwell) equations to the ones that involve the temporal evolution of the system, that is to say Equation 1.1.4 and Equation 1.1.5. Integrate these two sets of equations is known as the Vlasov-Maxwell formalism.

Furthermore, it is imperative for the purpose and treatment used in this work point out the nature of the Vlasov equation and its implications in the quasilinear theory that will be discussed in the following sections.

1.2 Kinetic formalism structure

Klimontovich [21] described the nature of N grained point particles, each possessing a charge q, mass m, and an average density n. Each obey its own trajectory $\boldsymbol{x}_i(t) \equiv [\boldsymbol{r}_i(t), \boldsymbol{v}_i(t)]$ in the space of positions resulting in its own microscopic density $N(\boldsymbol{x},t)$. Thus, elaborating a microscopic distribution function that satisfies the known continuity equation, we get

$$\frac{\partial N}{\partial t} + \boldsymbol{v} \cdot \frac{\partial N}{\partial \boldsymbol{r}} + \dot{\boldsymbol{v}} \cdot \frac{\partial N}{\partial \boldsymbol{v}} = 0. \tag{1.2.1}$$

It is clear to see that $\dot{\boldsymbol{v}}$ represents the acceleration, in this context, the Lorentz force.

$$\dot{\boldsymbol{v}} = \frac{q}{m}\left[\boldsymbol{E}(\boldsymbol{r},t) + \frac{\boldsymbol{v}}{c} \times \boldsymbol{B}(\boldsymbol{r},t)\right]. \tag{1.2.2}$$

Let us declare that the terms referred as the electric $\boldsymbol{E}(\boldsymbol{r},t)$ and magnetic field $\boldsymbol{B}(\boldsymbol{r},t)$ implicitly have the information either for the sources and the particles, whose solution for this microscopic fields are determined by the Maxwell equations in the electrostatic approximation. Where it emerges, what is called the *Klimontovich equation* [22].

$$\left[\frac{\partial}{\partial t} + L(\boldsymbol{x}) - \int V(\boldsymbol{x},\boldsymbol{x}')N(\boldsymbol{x}',t)d\boldsymbol{x}'\right] N(\boldsymbol{x}',t) = 0. \tag{1.2.3}$$

Where $L(\boldsymbol{x})$ is a single-particle operator defined by

$$L(\boldsymbol{x}) \equiv \boldsymbol{v}\cdot\frac{\partial}{\partial \boldsymbol{r}} + \frac{q}{m}\left(\boldsymbol{E}(\boldsymbol{r},t) + \frac{\boldsymbol{v}\times\boldsymbol{B}(\boldsymbol{r},t)}{c}\right)\cdot\frac{\partial}{\partial \boldsymbol{v}}, \tag{1.2.4}$$

and $V(\boldsymbol{x},\boldsymbol{x}')$ arise as a two-particle operator from the Coulomb interaction in an arbitrary volume, non-relevant for this explanation. Now, $\boldsymbol{E}(\boldsymbol{r},t)$ and $\boldsymbol{B}(\boldsymbol{r},t)$ in Equation 1.2.4 are the external fields, rather than include intrinsic to the point particles as we said previously. Even though it is already clear in Equation 1.1.1, this distinction will be helpful in the subsequent construction of the formalism.

A vital step into this theory is to relate the grained quantities with the macroscopic properties observed in the real world. Similarly, we average the microstates behavior over the phase space Γ taking the elements of the ensemble theory and Liouville's theorem.

Liouville's theorem gives the dynamics of a system of N particles that have $3N$ canonical coordinates and $3N$ conjugate momenta that are described in the Hamilton formalism, which yields the motion equations of an arbitrary $s-$distribution function in a $6N-$dimensional phase space.
If each point in the phase space represents a state of the system, whose number does not change in time as if they form an *incompressible fluid*, we may imply conservation of energy as a first rough approach. Consequently,

$$\frac{\partial \rho}{\partial t} + \nabla\cdot(\rho\boldsymbol{v}) = 0. \tag{1.2.5}$$

Where the velocity of this Hamiltonian flow is $\boldsymbol{v} = (\dot{p}_1,\ldots,\dot{p}_{3N};\dot{q}_1,\ldots,\dot{q}_{3N})$ and the nabla operator goes as $\nabla = (\partial/\partial p_1,\ldots,\partial p_{3N};\partial/\partial q_1,\ldots\partial/\partial q_{3N})$. Here, $\rho(q,p;t)$ represents the phase space density which obeys the Liouville distribution function and satisfies the normalization condition [23].

We can take, for instance, an average over the initial distribution of a physical quantity $f(q,p)$ where it has been proven [22], that at $t=0$:

$$\langle N(\boldsymbol{x}, t)\rangle = f_1(\boldsymbol{x}, t). \tag{1.2.6}$$

It has been obtained the single-particle distribution function. Additionally, one can perform $n-$particle averages to obtain a joint distribution function $f_s(\boldsymbol{x}, \boldsymbol{x}', \ldots \boldsymbol{x}^{s-1}; t)$ involves an arbitrary number (s) of particles.

1.2.1 BBGKY and Vlasov cumulant hierarchy

The Bogoliubov–Born–Green–Kirkwood–Yvon (BBGKY) hierarchy equations arises from this scheme of averaging many-particle distribution functions as a product of Equation 1.2.3 under the mechanical statistics considerations previously made [24, 25]. That is to say,

$$\left[\frac{\partial}{\partial t} + L(1)\right] N(1, t) = \int V(1, 2) N(1, t) N(2, t) d2. \tag{1.2.7}$$

Where we have adopted numeral notation instead of $\boldsymbol{x}, \boldsymbol{x}', \boldsymbol{x}''$, etc. Since we want to study a many-particle dynamics and it is less tedious. We may work likewise and extend for an arbitrary function $y(1, 2, \ldots; t)$ [22], resulting in

$$\left[\frac{\partial}{\partial t} + \sum_{i=1}^{s} L(i) - \frac{1}{n}\sum_{i\neq 1}^{s} V(i, j)\right] f_s(1, \ldots, s; t) = \sum_{i=1}^{s} \int V(i, s+1) f_{s+1}(1, \ldots, s+1; t) d(s+1). \tag{1.2.8}$$

Where $i \equiv (\boldsymbol{r}_i, \boldsymbol{v}_i)$ is the position and velocity of the $i-$th particle for an $f_s(1, \ldots, s)$ particle distribution function.

Let us notice that this scheme of averaging leads us to a set of coupled equations that clearly demonstrates that does not close in itself. The equation for the single-particle distribution depends on the two-particle distribution, the two-particle distribution requires of the three-particle distribution and so forth. Hence, we need a method of truncating this non-converging series of equations.

It is proposed an ansatz for Equation 1.2.8, a s single-particle distribution function of zeroth order in the discrete plasma parameter ($g \equiv 1/n\lambda_D^3$) limit through a power-series expansion.

$$f_s = f_s^{(0)} + f_s^{(1)} + f_s^{(2)} + \ldots. \tag{1.2.9}$$

Resulting in

$$\left[\frac{\partial}{\partial t} + L(1) - \int V(1,2)F(2,t)d2\right] F(1,t) = 0. \tag{1.2.10}$$

In a more conventional way, this expression may be rewritten and turn into Equation 1.1.1, known as the *Vlasov equation* or the *Boltzmann collisionless equation.*

Equation 1.1.1, now known as the Vlasov equation, inherits the same characteristics and challenges of the formalism it is based on. Like Liouville's theorem, it describes a conservative system—in this case, a collisionless plasma—so it also has time invariance, meaning the density of particles in phase space remains constant over time.

To address the problem analytically, we adopt a perturbative method that requires truncation of both the velocity distribution function $f(\boldsymbol{x}, \boldsymbol{v}, t)$ and the electromagnetic fields $\boldsymbol{E}(\boldsymbol{x}, t)$ and $\boldsymbol{B}(\boldsymbol{x}, t)$. From now on, the equilibrium distribution will be denoted by $F_\mu(\boldsymbol{x}, \boldsymbol{v}, t)$, while perturbations are expressed as $\delta^n f_\mu$. Each perturbative term depends recursively on higher-order corrections, giving rise to a correlation hierarchy. As a result, the Vlasov equation can support highly nonlinear solutions if these higher-order terms are included. While linear theory (first-order perturbations) is well studied, current research increasingly focuses on exploring the nonlinear dynamics through computational and numerical methods.

Analogously to the BBGKY hierarchy, R. C. Davidson [26] proposed a statistical framework for weakly turbulent plasma theory, which he termed the **cumulant hierarchy**. This approach describes the evolution of collective correlations in a Vlasov ensemble, a process now understood to arise naturally when this equation is solved perturbatively. In this way, we introduce a key concept that remains central to physics research, such as turbulence, which is particularly intriguing in a weakly turbulent regime. In this context, where discrete particle interactions are absent ($g \to 0$), turbulence is understood as a large number of random collective oscillations capable of excitation in the presence of an instability and weakly denotes that the average energy of the fields is comparatively smaller than the average kinetic energy of the particles. Yet, it is not a different formalism or approach, but a particular case of the BBGKY hierarchy that already contains a strong framework for turbulence. The *Vlasov Cumulant Hierarchy* just provides a practical way of describing as small correlations as s increases.

Based on the previous arguments, correlations containing information about multiwave and multiwave-particle interactions will be neglected. Following the approach outlined [26], we truncate the cumulant hierarchy to a two-body correlation function. Assuming sufficiently small finite wave amplitudes near the proton gyrofrequency, only the slow temporal response significantly influences the zero-order velocity distribution in a spatially homogeneous plasma, which governs energy transfer and the kinetic energy gained by particles [27].

Consequently, since we aim to solve the Vlasov equation using a first-order perturbative method, the framework we adopt is not strictly nonlinear. From this point on, we shall refer to this approach as *quasilinear moment theory*. Moreover, as previously noted, Equation 1.1.1 is inherently conservative. Within this quasilinear methodology, it is essential to verify that this conservation property is preserved. In fact, the conservation of particle number, energy, and momentum is satisfied [11].

1.3 Equilibrium condition

Based on the discussion in the previous section, we will define our equilibrium condition by introducing a first-order perturbation to the system that remains time-invariant. Setting the coordinate system such that $\boldsymbol{B} = \boldsymbol{B_0}\hat{z}$ and omitting all time-dependent perturbative terms, as well as for the distribution f_μ, and the fields $\boldsymbol{E}$ and $\boldsymbol{B}$ in Equation 1.1.1. Therefore, that the physical system is time-independent, current-free, and neutral. This leads to the zeroth-order Vlasov equation:

$$(\boldsymbol{v} \times \boldsymbol{\Omega}_\mu) \cdot \frac{\partial F_\mu}{\partial \boldsymbol{v}} = 0. \tag{1.3.1}$$

It is defined $\Omega_\mu = q_\mu B_0/m_\mu c$ and since it goes across the $\hat{z}-$direction, we provide it of a vector feature. The recently established implies that any zeroth-order distribution F_μ must satisfy as well

$$F_\mu(\boldsymbol{v}) = F_\mu(v_\perp, v_z). \tag{1.3.2}$$

In order to keep a proper coordinate system, we will define velocity $\boldsymbol{v}$ with cylindrical symmetry of motion. Thus similarly,

$$\frac{\partial F_\mu}{\partial \boldsymbol{v}} = \frac{\partial F_\mu}{\partial v_\perp}\hat{r} + \frac{1}{v_\perp}\frac{\partial F_\mu}{\partial \phi}\hat{\phi} + \frac{\partial F_\mu}{\partial v_z}\hat{z}. \tag{1.3.3}$$

Replacing in it into the equilibrium condition, equation (1.3.1),

$$-\Omega_\mu \frac{\partial F_\mu}{\partial \phi} = 0. \tag{1.3.4}$$

It is concluded that F_μ is independent respect to the azimuthal coordinate ϕ, meaning, **gyrotropic**. This is a necessary condition for study or compute quantities related to the distribution in equilibrium and free energy sources for microinstabilities [28] and may drive, among others, instabilities by temperature anisotropies.

1.4 Slow and Fast Dynamics of a Velocity Distribution Function

1.4.1 Linear theory

Since Equation 1.1.1 cannot be solved through a closed-formed solution, a perturbative method has been widely implemented where we consider first order perturbations. The distribution and fields develop according to

$$f_\mu = F_\mu(\boldsymbol{v}, t) + \delta f_\mu(\boldsymbol{x}, \boldsymbol{v}, t), \tag{1.4.1}$$

$$\boldsymbol{B} = B_0 \hat{z} + \delta \boldsymbol{B}, \tag{1.4.2}$$

$$\boldsymbol{E} = \delta \boldsymbol{E}. \tag{1.4.3}$$

Where in parallel propagation $\boldsymbol{k} = k_\parallel \hat{z}$ the perturbed quantities are written as Fourier-Laplace transformations.

$$\delta f_{\mu k} = \frac{1}{\sqrt{2\pi}} \int_0^{+\infty} dt \int_{-\infty}^{+\infty} dz \delta f_\mu \exp\{-i[kz - \omega t]\}, \tag{1.4.4}$$

$$\delta \boldsymbol{E}_k = \frac{1}{\sqrt{2\pi}} \int_0^{+\infty} dt \int_{-\infty}^{+\infty} dz \delta \boldsymbol{E} \exp\{-i[kz - \omega t]\}, \tag{1.4.5}$$

$$\delta \boldsymbol{B}_k = \frac{1}{\sqrt{2\pi}} \int_0^{+\infty} dt \int_{-\infty}^{+\infty} dz \delta \boldsymbol{B} \exp\{-i[kz - \omega t]\}. \tag{1.4.6}$$

Equally, Maxwell equations yield

$$ic\boldsymbol{k} \times \delta \boldsymbol{E}_k = i\omega \delta \boldsymbol{B}_k + \delta \boldsymbol{B}_k(0), \tag{1.4.7}$$

$$ic\boldsymbol{k} \times \delta \boldsymbol{B}_k = -i\omega \delta \boldsymbol{E}_k - \delta \boldsymbol{E}_k(0) + 4\pi \delta \boldsymbol{J}_k, \tag{1.4.8}$$

$$ic\boldsymbol{k} \cdot \delta \boldsymbol{B}_k = 0, \tag{1.4.9}$$

$$ic\boldsymbol{k} \cdot \delta \boldsymbol{E}_k = 4\pi \rho_k. \tag{1.4.10}$$

This way and using Faraday's law of magnetic induction, Equation 1.1.1 turns into

$$\Omega_\mu \frac{\partial \delta f_{\mu k}}{\partial \phi} + i(\omega - k v_\parallel)\delta f_{\mu k} = \frac{q_\mu}{m_\mu}\left[\delta \boldsymbol{E}_k + \frac{\boldsymbol{v}}{\omega} \times (\boldsymbol{k} \times \delta \boldsymbol{E}_k) + i\frac{\boldsymbol{v}}{c\omega} \times \delta \boldsymbol{B}_k(0)\right] \cdot \frac{\partial F_\mu}{\partial \boldsymbol{v}} - \delta f_{\mu k}(0). \tag{1.4.11}$$

This is a first-order differential equation for $\delta f_{\mu k}$, whose solution is

$$\delta f_{\mu k} = \tilde{f}_\mu(0) + \frac{1}{\Omega_\mu}\frac{q_\mu}{m_\mu}\int^\phi d\phi' e^{i\frac{\omega - v_\parallel k}{\Omega_\mu}(\phi - \phi')}\left[\delta \boldsymbol{E}_k + \frac{\boldsymbol{v}}{\omega} \times (\boldsymbol{k} \times \delta \boldsymbol{E}_k)\right] \cdot \frac{\partial F_\mu}{\partial \boldsymbol{v}}. \tag{1.4.12}$$

With its respective initial condition solution

$$\tilde{f}_\mu(0) = \frac{1}{\Omega_\mu}\frac{q_\mu}{m_\mu}\int^\phi d\phi' e^{i\frac{\omega - v_\parallel k}{\Omega_\mu}(\phi - \phi')}\left[i\frac{\boldsymbol{v}}{c\omega} \times \delta \boldsymbol{B}_k(0) \cdot \frac{\partial F_\mu}{\partial \boldsymbol{v}} - \delta f_{\mu k}(0)\right]. \tag{1.4.13}$$

On the other hand, due to cylindrical symmetry of motion

$$\boldsymbol{v} = v_\perp \cos\phi \hat{x} + v_\perp \sin\phi \hat{y} + v_\parallel \hat{z}. \tag{1.4.14}$$

This way,

$$\begin{aligned}\left[\delta \boldsymbol{E}_k + \frac{\boldsymbol{v}}{\omega} \times (\boldsymbol{k} \times \delta \boldsymbol{E}_k)\right] \cdot \frac{\partial F_\mu}{\partial \boldsymbol{v}} &= \frac{1}{\omega}\left[\delta \boldsymbol{E}_k(\omega - v_\parallel k_\parallel) + (\boldsymbol{v} \cdot \delta \boldsymbol{E}_k)\boldsymbol{k}\right] \cdot \frac{\partial F_\mu}{\partial \boldsymbol{v}}, \\ &= \lambda_\mu \delta E_{kx} \cos\phi + \lambda_\mu \delta E_{yx} \sin\phi + \delta E_{kz}\frac{\partial F_\mu}{\partial v_\parallel}.\end{aligned} \tag{1.4.15}$$

Where

$$\lambda_\mu = \frac{1}{\omega}\left\{(\omega - v_\parallel k_\parallel)\frac{\partial F_\mu}{\partial v_\perp} + v_\perp k \frac{\partial F_\mu}{\partial v_\parallel}\right\}. \tag{1.4.16}$$

Integrating explicitly, and defining $\eta_\mu^{(\sigma)} = (\omega - v_\parallel k + \sigma\Omega_\mu)/\Omega_\mu = \eta_\mu^{(0)} + \sigma$ and $\delta E_k^{(\pm)} = \frac{1}{2}(\delta E_{kx} \pm i\delta E_{ky})$, we obtain

$$\begin{aligned}
\delta f_{\mu k} &= \tilde{f}_\mu(0) + \frac{1}{\Omega_\mu}\frac{q_\mu}{m_\mu}\int^{\phi} d\phi' e^{i\frac{\omega - v_\parallel k}{\Omega_\mu}(\phi-\phi')}\left[\lambda_\mu \delta E_{kx}\cos\phi + \lambda_\mu\delta E_{yx}\sin\phi + \delta E_{kz}\frac{\partial F_\mu}{\partial v_\parallel}\right], \\
&= \tilde{f}_\mu(0) + \frac{1}{\Omega_\mu}\frac{q_\mu}{m_\mu}e^{-i\eta_\mu^{(0)}\phi}\int^{\phi} d\phi'\left[\lambda_\mu e^{-i\eta_\mu^{(+)}\phi'}\delta E_k^{(-)} + \lambda_\mu e^{-i\eta_\mu^{(-)}\phi'}\delta E_k^{(+)} + e^{i\eta_\mu^{(0)}\phi'}\delta E_{kz}\frac{\partial F_\mu}{\partial v_\parallel}\right], \\
&= \tilde{f}_\mu(0) + \frac{1}{\Omega_\mu}\frac{q_\mu}{m_\mu}\left[\lambda_\mu\frac{e^{i\phi}}{i\eta_\mu^{(+)}}\delta E_k^{(-)} + \lambda_\mu\frac{e^{-i\phi}}{i\eta_\mu^{(-)}}\delta E_k^{(+)} + \frac{1}{i\eta_\mu^{(0)}}\delta E_{kz}\frac{\partial F_\mu}{\partial v_\parallel}\right], \\
&= \tilde{f}_\mu(0) - i\frac{q_\mu}{m_\mu}\left[\lambda_\mu\frac{e^{i\phi}\delta E_k^{(-)}}{\omega - v_\parallel k + \Omega_\mu} + \lambda_\mu\frac{e^{-i\phi}\delta E_k^{(+)}}{\omega - v_\parallel k - \Omega_\mu} + \frac{\delta E_{kz}}{\omega - v_\parallel k}\frac{\partial F_\mu}{\partial v_\parallel}\right].
\end{aligned} \tag{1.4.17}$$

1.4.2 Dielectric tensor and dispersion relations

The dielectric tensor is how we characterize the response of the conducting media to any perturbation that may happen. Here, we construct it using the relevant and necessary Maxwell equations in their Fourier-Laplace transformation form.

$$ic\boldsymbol{k} \times \delta\boldsymbol{E}_k = i\omega\delta\boldsymbol{B}_k + i\omega\delta\boldsymbol{B}_k(0), \tag{1.4.18}$$

$$ic\boldsymbol{k} \times \delta\boldsymbol{B}_k = -i\omega\delta\boldsymbol{E}_k - i\omega\delta\boldsymbol{E}_k(0) + 4\pi\delta\boldsymbol{J}_k. \tag{1.4.19}$$

Where

$$\delta\boldsymbol{J}_k = \sum_\mu q_\mu n_\mu \int d^3v\boldsymbol{v}\delta f_{\mu k}. \tag{1.4.20}$$

Solving for $\delta \boldsymbol{B}_k$ in Equation 1.4.18 and replacing it in Equation 1.4.19, we get

$$
\begin{aligned}
ic\boldsymbol{k} \times (ic\boldsymbol{k} \times \delta \boldsymbol{E}_k - \delta \boldsymbol{B}_k(0)) = \omega^2 \delta \boldsymbol{E}_k - i\omega \delta \boldsymbol{E}_k(0) + 4\pi i \omega \sum_\mu q_\mu n_\mu \int d^3v \boldsymbol{v} \delta f_{\mu k}, \\
c^2 \boldsymbol{k}^2 \times (\boldsymbol{k} \times \delta \boldsymbol{E}_k) + \omega^2 \delta \boldsymbol{E}_k = -ic\boldsymbol{k} \times \delta \boldsymbol{B}_k(0) + i\omega \delta \boldsymbol{E}_k(0) - 4\pi i \omega \sum_\mu q_\mu n_\mu \int d^3v \boldsymbol{v} \delta f_{\mu k}, \\
\left(1 - \frac{c^2k^2}{\omega^2}\right) \delta \boldsymbol{E}_k + \frac{c^2}{\omega^2} \boldsymbol{k}(\boldsymbol{k} \cdot \delta \boldsymbol{E}_k) = -\frac{4\pi i}{\omega} \delta \boldsymbol{J}_k(0) - 4\pi \sum_\mu \check{\chi}_\mu \cdot \delta \boldsymbol{E}_k.
\end{aligned}
\tag{1.4.21}
$$

Where,

$$
\delta \boldsymbol{J}_k(0) = \frac{1}{4\pi\omega} c\boldsymbol{k} \times \delta \boldsymbol{B}_k(0) - \frac{1}{4\pi} \delta \boldsymbol{E}_k(0) + \sum_\mu q_\mu n_\mu \int d^3v \boldsymbol{v} f_\mu(0). \tag{1.4.22}
$$

Thus,

$$
\check{\chi}_\mu \cdot \delta \boldsymbol{E}_k = \frac{q_\mu^2 n_\mu}{m_\mu \omega} \int d^3v \boldsymbol{v} \left[\lambda_\mu \frac{e^{i\phi} \delta E_k^{(-)}}{\omega - v_\parallel k + \Omega_\mu} + \lambda_\mu \frac{e^{i\phi} \delta E_k^{(+)}}{\omega - v_\parallel k - \Omega_\mu} + \frac{\delta E_{kz}}{\omega - v_\parallel k} \frac{\partial F_\mu}{\partial v_\parallel} \right] \tag{1.4.23}
$$

Integrating explicitly respect to ϕ,

$$
\begin{aligned}
\check{\chi}_\mu \cdot \delta \boldsymbol{E}_k &= \frac{\omega_{p\mu}^2}{4\pi\omega} \int dv_\perp dv_\parallel d\phi v_\perp \begin{pmatrix} v_\perp \cos\phi \\ v_\perp \sin\phi \\ v_\parallel \end{pmatrix} \left[\lambda_\mu \frac{e^{i\phi} \delta E_k^{(-)}}{\omega - v_\parallel k + \Omega_\mu} + \lambda_\mu \frac{e^{i\phi} \delta E_k^{(+)}}{\omega - v_\parallel k - \Omega_\mu} + \frac{\delta E_{kz}}{\omega - v_\parallel k} \frac{\partial F_\mu}{\partial v_\parallel} \right], \\
&= \frac{\omega_{p\mu}^2}{4\pi\omega} \int dv_\perp dv_\parallel d\phi v_\perp \begin{pmatrix} \frac{v_\perp}{2} \lambda_\mu \left[\frac{\delta E_k^{(+)}}{\omega - v_\parallel k - \Omega_\mu} + \frac{\delta E_k^{(-)}}{\omega - v_\parallel k + \Omega_\mu} \right] \\ \frac{v_\perp}{2i} \lambda_\mu \left[\frac{\delta E_k^{(+)}}{\omega - v_\parallel k - \Omega_\mu} - \frac{\delta E_k^{(-)}}{\omega - v_\parallel k + \Omega_\mu} \right] \\ v_\parallel \frac{\delta E_{kz}}{\omega - v_\parallel k} \frac{\partial F_\mu}{\partial v_\parallel} \end{pmatrix}.
\end{aligned}
\tag{1.4.24}
$$

We can define the susceptibility, in cartesian coordinates, where due parallel propagation this tensor takes the form

$$\check{\chi}_\mu = \begin{pmatrix} \chi_\mu^{xx} & \chi_\mu^{xy} & 0 \\ -\chi_\mu^{xy} & \chi_\mu^{xx} & 0 \\ 0 & 0 & \chi_\mu^{zz} \end{pmatrix},$$

$$= \frac{\omega_{p\mu}^2}{2\omega}\int dv_\perp dv_\parallel v_\parallel \begin{pmatrix} \frac{v_\perp}{4}\left[\frac{\lambda_\mu}{\omega - v_\parallel k - \Omega_\mu} + \frac{\lambda_\mu}{\omega - v_\parallel k + \Omega_\mu}\right] & \frac{v_\perp}{4i}\left[\frac{\lambda_\mu}{\omega - v_\parallel k + \Omega_\mu} - \frac{\lambda_\mu}{\omega - v_\parallel k - \Omega_\mu}\right] & 0 \\ -\frac{v_\perp}{4i}\left[\frac{\lambda_\mu}{\omega - v_\parallel k + \Omega_\mu} - \frac{\lambda_\mu}{\omega - v_\parallel k - \Omega_\mu}\right] & \frac{v_\perp}{4}\left[\frac{\lambda_\mu}{\omega - v_\parallel k - \Omega_\mu} + \frac{\lambda_\mu}{\omega - v_\parallel k + \Omega_\mu}\right] & 0 \\ 0 & 0 & \frac{v_\parallel}{\omega - v_\parallel k}\frac{\partial F_\mu}{\partial v_\parallel} \end{pmatrix}, \tag{1.4.25}$$

where $\chi^{(\pm)\mu} = \chi_\mu^{xx} \pm i\chi_\mu^{yy}$, and

$$\chi_\mu^{(\pm)} = \frac{\omega_{p\mu}^2}{4\omega}\int dv_\perp dv_\parallel \frac{v_\perp^2 \lambda_\mu}{\omega - v_\parallel k \pm \Omega_\mu},$$

$$= \frac{\omega_{p\mu}^2}{4\omega^2}\int dv_\perp dv_\parallel \frac{v_\perp^2}{\omega - v_\parallel k \pm \Omega_\mu}\left[(\omega - \boldsymbol{v}\cdot\boldsymbol{k})\frac{\partial F_\mu}{\partial v_\perp} + v_\perp k \frac{\partial F_\mu}{\partial v_\parallel}\right], \tag{1.4.26}$$

$$\chi_\mu^{zz} = \frac{\omega_{p\mu}^2}{2\omega}\int dv_\perp dv_\parallel \frac{v_\perp v_\parallel}{\omega - v_\parallel k}\frac{\partial F_\mu}{\partial v_\parallel}. \tag{1.4.27}$$

Replacing into Equation 1.4.21,

$$\begin{pmatrix} 1 - \frac{c^2k^2}{\omega^2} + 4\pi\sum \chi_\mu^{xx} & 4\pi\sum_\mu \chi_\mu^{xy} & 0 \\ -4\pi\sum_\mu \chi_\mu^{xy} & 1 - \frac{c^2k^2}{\omega^2} + 4\pi\sum \chi_\mu^{xx} & 0 \\ 0 & 0 & 1 + 4\pi\sum_\mu \chi^{zz} \end{pmatrix}\begin{pmatrix} \delta E_{kx} \\ \delta E_{ky} \\ \delta E_{kz} \end{pmatrix} = -\frac{4\pi i}{\omega}\delta \boldsymbol{J}_k(0). \tag{1.4.28}$$

Non-trivial solutions of this equations are the normal modes of the system, which satisfy the dispersion relation —determinant of the matrix shown above is zero— given by

$$\left[1 + 4\pi\sum_\mu \chi_\mu^{zz}\right]\left[\left(1 - \frac{c^2k^2}{\omega^2} + 4\pi\sum \chi_\mu^{xx}\right)^2 + \left(4\pi\sum_\mu \chi_\mu^{xy}\right)^2\right] = 0,$$

$$\left[1 + 4\pi\sum_\mu \chi_\mu^{zz}\right]\left[1 - \frac{c^2k^2}{\omega^2} + 4\pi\sum \chi_\mu^{(+)}\right]\left[1 - \frac{c^2k^2}{\omega^2} + 4\pi\sum \chi_\mu^{(-)}\right] = 0. \tag{1.4.29}$$

The frequency of longitudinal modes ($\delta E_{kz} = 0$) are given by

$$1 + 4\pi \sum_{\mu} \chi_{\mu}^{zz} = 0,$$

$$1 + 2\pi \sum \frac{\omega_{p\mu}^2}{\omega} \int dv_{\perp} dv_{\parallel} \frac{v_{\perp} v_{\parallel}}{\omega - v_{\parallel k}} \frac{\partial F_{\mu}}{\partial v_{\parallel}} = 0. \tag{1.4.30}$$

Similarly, the frequency of transverse modes ($\delta E_{kx} = \delta E_{ky} = 0$) are given by

$$1 - \frac{c^2 k^2}{\omega^2} + \pi \sum_{\mu} \frac{\omega_{p\mu}^2}{\omega^2} \int dv_{\perp} dv_{\parallel} \frac{v_{\perp}^2}{\omega - v_{\parallel} k \pm \Omega_{\mu}} \left[(\omega - \boldsymbol{v} \cdot \boldsymbol{k}) \frac{\partial F_{\mu}}{\partial v_{\perp}} + v_{\perp} k \frac{\partial F_{\mu}}{\partial v_{\parallel}} \right] = 0. \tag{1.4.31}$$

1.4.3 Quasilinear theory

Linear theory is able to predict the growth or damping of waves, a clear example of this are kinetic microinstabilities in the system (Alfvén-cyclotron, firehose, electroacoustic, etc.) or Landau damping. However, when we have resonant interactions between waves due to inherent plasma dynamical behavior, a balance in energy between particles and the electromagnetic fields in the system is implied and so that linear theory becomes ineffectual; energy conservation theorems are nonlinear since $W_{EM} \propto (E^2 + B^2)/8\pi$ [11]. Therefore, turn to a theory that considers this physical principle is essential. For this study, the wave-particle interaction is considered, meaning, $\omega \pm \Omega_{\mu} = k_z v_z$.

We will employ the same Vlasov equation by the same perturbative method as made in the previous section where second order perturbations will not be neglected this time. Thus,

$$\frac{\partial F_{\mu}}{\partial t} + (\boldsymbol{v} \times \boldsymbol{\Omega}_{\mu}) \cdot \frac{\partial F_{\mu}}{\partial \boldsymbol{v}} + \delta \boldsymbol{a}_{\mu} \cdot \frac{\partial F_{\mu}}{\partial \boldsymbol{v}} = - \left[\frac{\partial \delta f_{\mu}}{\partial t} + \boldsymbol{v} \cdot \frac{\partial \delta f_{\mu}}{\partial \boldsymbol{x}} + (\boldsymbol{v} \times \boldsymbol{\Omega}_{\mu}) \cdot \frac{\partial \delta f_{\mu}}{\partial \boldsymbol{v}} + \delta \boldsymbol{a}_{\mu} \cdot \frac{\partial \delta f_{\mu}}{\partial \boldsymbol{v}} \right]. \tag{1.4.32}$$

Where

$$\delta \boldsymbol{a}_{\mu} = \frac{q_{\mu}}{m_{\mu}} \left(\delta \boldsymbol{E} + \frac{\boldsymbol{v}}{c} \times \delta \boldsymbol{B} \right). \tag{1.4.33}$$

And $F_{\mu}(\boldsymbol{v}, t)$ is the averaged distribution for a spatially uniform plasma, defined clasically as

$$F_{\mu}(\boldsymbol{v}, t) = \langle f_{\mu} \rangle = \frac{1}{V} \int d^3 r f_{\mu}(\boldsymbol{r}, \boldsymbol{v}, t). \tag{1.4.34}$$

Averaging Equation 1.4.32, it is obtained its correlation. Consequently,

$$\frac{\partial \delta f_\mu}{\partial t} + \boldsymbol{v} \cdot \frac{\partial \delta f_\mu}{\partial \boldsymbol{x}} + (\boldsymbol{v} \times \boldsymbol{\Omega}_\mu) \cdot \frac{\partial \delta f_\mu}{\partial \boldsymbol{v}} + \delta \boldsymbol{a}_\mu \cdot \frac{\partial \delta f_\mu}{\partial \boldsymbol{v}} = \left\langle \delta \boldsymbol{a}_\mu \cdot \frac{\partial \delta f_\mu}{\partial \boldsymbol{v}} \right\rangle - \delta \boldsymbol{a}_\mu \cdot \frac{\partial \delta f_\mu}{\partial \boldsymbol{v}}. \tag{1.4.35}$$

This expression leads us to the same linear dispersion relation shown in the previous section under the same assumptions and approximations. Still, considering second order perturbations allow us to talk about two different time scales in the system and treat them by their own behaviour, a slow one where the linear dispersion relations are put up into, and a faster one where fluctuations matters.

On one hand, the equation for F_μ yields

$$\begin{aligned} \frac{\partial F_\mu}{\partial t} &= -\frac{q_\mu}{m_\mu} \left\langle \left(\delta \boldsymbol{E} + \frac{\boldsymbol{v}}{c} \times \boldsymbol{B} \right) \cdot \frac{\partial \delta f_\mu}{\delta \boldsymbol{v}} \right\rangle, & (1.4.36) \\ &= -\frac{q_\mu}{m_\mu} \frac{1}{L} \int dz \left(\delta \boldsymbol{E} + \frac{\boldsymbol{v}}{c} \times \boldsymbol{B} \right) \cdot \frac{\partial \delta f_\mu}{\delta \boldsymbol{v}}. & (1.4.37) \end{aligned}$$

Following the averaged distribution definition and by $(\boldsymbol{v} \times \boldsymbol{\Omega}) \cdot \partial F_\mu / \partial \boldsymbol{v} = -\Omega_\mu \partial F_\mu / \partial \phi = 0$ and the inverse Fourier-Laplace transforms for the VDF and electric and magnetic field, we get

$$\begin{aligned} \frac{\partial F_\mu}{\partial t} &= -\frac{q_\mu}{m_\mu} \frac{1}{L} \int_{-\infty}^{\infty} dk' \int_{-\infty}^{\infty} dk \left(\delta \boldsymbol{E} + \frac{\boldsymbol{v}}{c} \times \boldsymbol{B} \right) \cdot \frac{\partial \delta f_{\mu k}}{\delta \boldsymbol{v}} \frac{1}{2\pi} \int dz e^{i(k+k')z} e^{-i(\omega_k + \omega_k)t}, \\ &= -\frac{q_\mu}{m_\mu} \frac{1}{L} \int_{-\infty}^{\infty} dk' \int_{-\infty}^{\infty} dk \left(\delta \boldsymbol{E}_k + \frac{\boldsymbol{v}}{c} \times \boldsymbol{B}_k \right) \cdot \frac{\partial \delta f_{\mu k}}{\delta \boldsymbol{v}} \delta(k + k') e^{-i(\omega_k + \omega_k)t}, \\ &= -\frac{q_\mu}{m_\mu} \frac{1}{L} \int_{-\infty}^{\infty} dk \left(\delta \boldsymbol{E}_{-k} + \frac{\boldsymbol{v}}{c} \times \boldsymbol{B}_{-k} \right) \cdot \frac{\partial \delta f_{\mu k}}{\delta \boldsymbol{v}} e^{-i(\omega_k + \omega_{-k})t}. \end{aligned} \tag{1.4.38}$$

Then, using Faraday's law and neglecting its initial condition the temporal evolution of F_μ is

$$\frac{\partial F_\mu}{\partial t} = -\frac{q_\mu}{m_\mu} \frac{1}{L} \int_{-\infty}^{\infty} dk \left(\delta \boldsymbol{E}_{-k} + \frac{\boldsymbol{v}}{\omega_{-k}} \times (\boldsymbol{k} \times \delta \boldsymbol{E}_{-k}) \right) \cdot \frac{\partial \delta f_{\mu k}}{\delta \boldsymbol{v}}. \tag{1.4.39}$$

1.4.4 Quasilinear moments

On the other, let us consider $\Psi(v_\perp, v_\parallel)$ be any scalar or vector function of the velocities gyrotropic. Thus, define the phase-space average

$$\langle\!\langle \Psi \rangle\!\rangle = \int dv_\perp dv_\parallel d\phi v_\perp \Psi(v_\perp, v_\parallel) F_\mu. \tag{1.4.40}$$

The temporal evolution of this function will be study by using Equation 1.4.39. Then,

$$\begin{aligned}
\frac{\partial \langle\!\langle \Psi \rangle\!\rangle}{\partial t} &= \int dv_\perp dv_\parallel d\phi v_\perp \Psi(v_\perp, v_\parallel) \frac{\partial F_\mu}{\partial t}, \\
&= -\frac{q_\mu}{m_\mu} \frac{1}{L} \int_{-\infty}^{\infty} dk \int dv_\perp dv_\parallel d\phi v_\perp \Psi(v_\perp, v_\parallel) \left(\delta \boldsymbol{E}_{-k} + \frac{\boldsymbol{v}}{c} \times (\boldsymbol{k} \times \delta \boldsymbol{B}_{-k}) \right) \cdot \frac{\partial \delta f_{\mu k}}{\delta \boldsymbol{v}} e^{-i(\omega_k + \omega_{-k})t}, \\
&= \frac{q_\mu}{m_\mu} \frac{1}{L} \int_{-\infty}^{\infty} dk \int dv_\perp dv_\parallel d\phi v_\perp \delta f_{\mu k} \frac{\partial \Psi}{\partial \boldsymbol{v}} \cdot \left(\delta \boldsymbol{E}_k + \frac{\boldsymbol{v}}{c} \times \delta \boldsymbol{B}_{-k} \right) e^{2\gamma_k t}.
\end{aligned} \tag{1.4.41}$$

Where we have used $\omega_{-k} = -\omega_k^*$ and $\mathrm{Im}(\omega_k) = \gamma(k)$. In addition, $c\boldsymbol{k} \times \delta \boldsymbol{E}_{-k} = -\omega_{-k} \delta \boldsymbol{B}_{-k}$, ignoring its initial condition,

$$\begin{aligned}
\frac{\partial \Psi}{\partial \boldsymbol{v}} \cdot \left(\delta \boldsymbol{E}_k + \frac{\boldsymbol{v}}{c} \times \delta \boldsymbol{B}_{-k} \right) &= \frac{\partial \Psi}{\partial \boldsymbol{v}} \cdot \left(\delta \boldsymbol{E}_{-k} - \frac{\boldsymbol{v}}{\omega_{-k}} \times (\boldsymbol{k} \times \delta \boldsymbol{E}_{-k}) \right), \\
&= \frac{1}{\omega_{-k}} \frac{\partial \Psi}{\partial \boldsymbol{v}} \cdot \left[(\omega_{-k} + v k_\parallel) \delta \boldsymbol{E}_{-k} - (\boldsymbol{v} \cdot \delta \boldsymbol{E}_{-k}) \boldsymbol{k} \right], \\
&= \Gamma_\Psi \cos\phi \delta E_{-kx} + \Gamma_\Psi \sin\phi \delta E_{-ky} + \frac{\partial \Psi}{\partial v_\parallel} \delta E_{-kz}, \\
&= \Gamma_\Psi \delta E_{-k}^{(+)} e^{i\phi} + \Gamma_\Psi \delta E_{-k}^{(-)} e^{-i\phi} + \frac{\partial F_\mu}{\partial v_\parallel} \delta E_{kz}.
\end{aligned} \tag{1.4.42}$$

Where, similarly to previous section

$$\Gamma_\Psi = \frac{1}{\omega_{-k}} \left[(\omega_{-k} + v_\parallel k) \frac{\partial \Psi}{\partial v_\perp} - v_\perp k \frac{\partial \Psi}{\partial v_\parallel} \right] \tag{1.4.43}$$

Replacing $\delta f_{\mu k}$ from Equation 1.4.17 and integrating explicitly with respect to ϕ, we get

$$
\begin{aligned}
\frac{\partial \langle\langle \Psi \rangle\rangle}{\partial t} &= \frac{q_\mu}{m_\mu}\frac{1}{L}\int_{-\infty}^{\infty} dk \int dv_\perp dv_\parallel d\phi v_\perp \delta f_{\mu k}\frac{\partial \Psi}{\partial \boldsymbol{v}}\cdot\left(\delta \boldsymbol{E}_k + \frac{\boldsymbol{v}}{c}\times \delta \boldsymbol{B}_{-k}\right)e^{2\gamma_k t}, \\
&= -\left(\frac{q_\mu}{m_\mu}\right)^2 \frac{2\pi i}{L}\int_{-\infty}^{\infty} dk \int dv_\perp dv_\parallel v_\perp \\
&\left[\lambda_\mu \frac{\Gamma_\Psi e^{i\phi}\delta E_{-k}^{(+)}\delta E_k^{(-)}}{\omega - v_\parallel k + \Omega_\mu} + \lambda_\mu \frac{\Gamma_\Psi e^{-i\phi}\delta E_{-k}^{(-)}\delta E_k^{(+)}}{\omega - v_\parallel k - \Omega_\mu} + \frac{\frac{\partial \Psi}{\partial v_\parallel}\delta E_{kz}\delta E_{-kz}}{\omega - v_\parallel k}\frac{\partial F_\mu}{\partial v_\parallel}\right]e^{2\gamma_k t}, \qquad (1.4.44)\\
&= -\left(\frac{q_\mu}{m_\mu}\right)^2 \frac{2\pi i}{L}\int_{-\infty}^{\infty} dk \int dv_\perp dv_\parallel v_\perp \\
&\left[\lambda_\mu \frac{\Gamma_\Psi |\delta E_k^{(-)}|^2}{\omega - v_\parallel k + \Omega_\mu} + \lambda_\mu \frac{\Gamma_\Psi |\delta E_k^{(+)}|^2}{\omega - v_\parallel k - \Omega_\mu} + \frac{\frac{\partial \Psi}{\partial v_\parallel}|\delta E_{kz}|^2}{\omega - v_\parallel k}\frac{\partial F_\mu}{\partial v_\parallel}\right]e^{2\gamma_k t}.
\end{aligned}
$$

Let us notice that for a fixed polarization, two of the last terms are zero implying that only the first term contributes in terms of energy. Thus, we can write a simplified equation:

$$
\frac{\partial \langle\langle v_\parallel \rangle\rangle}{\partial t} = -\left(\frac{q_\mu}{m_\mu}\right)^2 \frac{2\pi i}{L}\int_{-\infty}^{\infty} dk \int dv_\perp dv_\parallel v_\perp \left[\lambda_\mu \frac{\Gamma_\Psi |\delta E_k^{(\pm)}|^2}{\omega - v_\parallel k \mp \Omega_\mu} + \frac{\frac{\partial \Psi}{\partial v_\parallel}|\delta E_{kz}|^2}{\omega - v_\parallel k}\frac{\partial F_\mu}{\partial v_\parallel}\right]e^{2\gamma_k t}. \qquad (1.4.45)
$$

Therefore we can calculate less tediously the moments that are of our interest just by differentiating Γ_Ψ. Then, the first parallel moment or drift $\langle\langle v_\parallel \rangle\rangle$ we obtain $\Gamma_{v_\parallel} = v_\perp k/\omega_k^*$. Replacing into Equation 1.4.45,

$$
\begin{aligned}
\frac{\partial \langle\langle v_\parallel \rangle\rangle}{\partial t} &= -\left(\frac{q_\mu}{m_\mu}\right)^2 \frac{2\pi i}{L}\int_{-\infty}^{\infty} dk e^{2\gamma_k t}\int dv_\perp dv_\parallel v_\parallel \left[\lambda_\mu \frac{v_\perp k/\omega_k^* |\delta E_k^{(\pm)}|^2}{\omega - v_\parallel k \mp \Omega_\mu} + \frac{|\delta E_{kz}|^2}{\omega - v_\parallel k}\frac{\partial F_\mu}{\partial v_\parallel}\right], \\
&= -\left(\frac{q_\mu}{m_\mu}\right)^2 \frac{4\pi i}{L}\frac{1}{\omega_{p\mu}^2}\int_{-\infty}^{\infty} dk e^{2\gamma_k t}\left[\frac{2\omega_k^2}{c^2 k}\chi_\mu^{(\pm)}|\delta B_k^{(\pm)}|^2 + k\chi_\mu^{zz}|\delta E_{kz}|^2\right].
\end{aligned} \qquad (1.4.46)
$$

Where we have replaced $|\delta B_k^{(\pm)}|^2 = |ck\delta E_k^{(\pm)}/\omega_k|^2$, we have used the definition in Equation 1.4.26 and Equation 1.4.27 for susceptibilities $\chi_\mu^{(\pm)}$ and χ_μ^{zz}, respectively, such that

$$\int dv_\perp dv_\parallel \frac{v_\perp}{\omega_k - v_\parallel k}\frac{\partial F_\mu}{\partial v_\parallel} = \frac{2k}{\omega_{p\mu}^2}\chi_\mu^{zz}, \tag{1.4.47}$$

and used that F_μ vanishes for $v_\parallel \to \pm\infty$. Further calculations to this integral are included in the section A1.

The second parallel moment or parallel temperature $\langle\langle v_\parallel^2\rangle\rangle$ is obtained by taken $\Gamma_{v_\parallel^2} = 2kv_\perp v_\parallel/\omega_k^*$ and identically replacing into Equation 1.4.45,

$$\begin{aligned}
\frac{\partial\langle\langle v_\parallel^2\rangle\rangle}{\partial t} &= -\left(\frac{q_\mu}{m_\mu}\right)^2 \frac{4\pi i}{L}\int_{-\infty}^{\infty} dk e^{2\gamma_k t}\int dv_\perp dv_\parallel v_\perp \left[\frac{v_\parallel|\delta E_{kz}|^2}{\omega - v_\parallel k}\frac{\partial F_\mu}{\partial v_\parallel} + \lambda_\mu \frac{v_\perp k/\omega_k^* |\delta B_k^{(\pm)}|^2}{\omega - v_\parallel k \mp \Omega_\mu}\right], \\
&= -\left(\frac{q_\mu}{m_\mu}\right)^2 \frac{4\pi i}{L}\int_{-\infty}^{\infty} dk e^{2\gamma_k t}\int dv_\perp dv_\parallel v_\perp \left[\frac{2\omega_k}{\omega_{p\mu}^2}\chi_\mu^{zz}|\delta E_{kz}|^2 \ldots\right. \\
&\left. + \left(\frac{4\omega_k}{\omega_{p\mu}^2}(\omega_k \mp \Omega_\mu)\chi_\mu^{(\mp)} + \frac{\omega - \langle\langle v\rangle\rangle k}{\pi\omega_k}\right)\frac{\omega_k}{c^2k^2}|\delta B_k^{(\pm)}|^2\right].
\end{aligned} \tag{1.4.48}$$

Where we have replaced $|\delta B_k^{(\pm)}|^2 = |ck\delta E_k^{(\pm)}/\omega_k|^2$, we have used the definition shown in Equation 1.4.26 and Equation 1.4.27 for susceptibilities $\chi_\mu^{(\pm)}$ and χ_μ^{zz}, respectively, such that

$$\int dv_\perp dv_\parallel \lambda \frac{v_\perp^2 k v_\parallel}{\omega_k - v_\parallel k \mp \Omega_\mu} = (\omega_k \mp \Omega_\mu)\frac{4\omega_k}{\omega_{p\mu}^2}\chi_\mu^{\mp} + \frac{\omega_k - \langle\langle v_\parallel\rangle\rangle k}{\pi\omega_k}. \tag{1.4.49}$$

More details about this integral are shown in the section A1.

At last, the second transverse moment $\langle\langle v_\perp^2\rangle\rangle$ or transverse temperature. In this case, we have $\Gamma_{v_\perp^2} = 2v_\perp(\omega_k^* - v_\parallel k)/\omega_k^*$ that replacing into Equation 1.4.45.

$$\begin{aligned}
\frac{\partial\langle\langle v_\perp^2\rangle\rangle}{\partial t} &= -\left(\frac{q_\mu}{m_\mu}\right)^2 \frac{4\pi i}{L}\int_{-\infty}^{\infty} dk e^{2\gamma_k t}\int dv_\perp dv_\parallel \lambda_\mu \frac{v_\perp^2(\omega_k^* - v_\parallel k)}{\omega_k - v_\parallel k \mp \Omega_\mu}\frac{1}{\omega_k^*}|\delta E_k^{(\pm)}|^2, \\
&= -\left(\frac{q_\mu}{m_\mu}\right)^2 \frac{4\pi i}{L}\int_{-\infty}^{\infty} dk e^{2\gamma_k t}\frac{\omega_k}{c^2k^2}\int dv_\perp dv_\parallel \lambda_\mu v_\perp^2\left[\frac{\omega_k^* - \omega_k \pm \Omega_\mu}{\omega_k - v_\parallel k \mp \Omega_\mu} + 1\right]|\delta B_k^{(\pm)}|^2, \\
&= \left(\frac{q_\mu}{m_\mu}\right)^2 \frac{4\pi i}{L}\int_{-\infty}^{\infty} dk e^{2\gamma_k t}\frac{\omega_k}{c^2k^2}\left[(2i\gamma \mp \Omega_\mu)\frac{4\omega_k}{\omega_{p\mu}^2}\chi^{(\mp)} + \frac{\omega_k - \langle\langle v_\parallel\rangle\rangle k}{\pi\omega_k}\right]|\delta B_k^{(\pm)}|^2
\end{aligned} \tag{1.4.50}$$

1.4.5 Energy conservation

Temporal evolution of the total kinetic energy is given by

$$\begin{aligned}\frac{\partial K}{\partial t} &= \sum_{\mu}\frac{1}{2}m_\mu n_\mu\int d\phi dv_\perp dv_\parallel v_\perp(v_\perp^2+v_\parallel^2)\frac{\partial F_\mu}{\partial t},\\ &= \sum_{\mu}\frac{1}{2}m_\mu n_\mu\left(\frac{\partial\langle\langle v_\perp^2\rangle\rangle}{\partial t}+\frac{\partial\langle\langle v_\parallel^2\rangle\rangle}{\partial t}\right).\end{aligned} \tag{1.4.51}$$

Where we have replaced explicitly for $\partial\langle\langle v_\perp^2\rangle\rangle/\partial t$ and $\partial\langle\langle v_\parallel^2\rangle\rangle/\partial t$ according to the definition given in Equation 1.4.40. We factorize for the derivative terms,

$$\begin{aligned}\frac{\partial K}{\partial t} &= -\sum_{\mu}\frac{4\pi q_\mu^2 n_\mu}{m_\mu}\frac{i}{L}\int_{-\infty}^{\infty}dke^{2\gamma_k t}\frac{\omega_k}{\omega_{p\mu}^2}\left[2\chi_\mu^{(\mp)}|\delta E_k^{(\pm)}|^2+\chi_\mu^{zz}|\delta E_{kz}|^2\right],\\ &= -\frac{i}{L}\int_{-\infty}^{\infty}dke^{2\gamma_k t}\omega_k\sum_{\mu}\left[2\chi_\mu^{(\mp)}|\delta E_k^{(\pm)}|^2+\chi_\mu^{zz}|\delta E_{kz}|^2\right].\end{aligned} \tag{1.4.52}$$

Where $\omega_{p\mu}^2 = 4\pi q_\mu^2 n_\mu/m_\mu$ and from each dispersion relations we have that

$$\begin{aligned}4\pi\sum_{\mu}\chi_\mu^{(\pm)} &= c^2k^2/\omega^2-1,\\ 4\pi\sum_{\mu}\chi_\mu^{zz} &= -1.\end{aligned}$$

As follows,

$$\frac{\partial K}{\partial t} = \frac{i}{4\pi L}\int_{-\infty}^{\infty}dke^{2\gamma_k t}\omega_k\left[2\left(1-\frac{c^2k^2}{\omega_k^2}\right)|\delta E_k^{(\pm)}|^2+|\delta E_{kz}|^2\right] \tag{1.4.53}$$

Since $\omega = \omega_r + i\gamma$, it is true that $\omega_{-k} = -\omega_k^*$ meaning that the real part is odd, so we write

$$
\begin{aligned}
\frac{\partial K}{\partial t} &= -\frac{1}{4\pi L}\int_{-\infty}^{\infty} dk e^{2\gamma_k t}\gamma_k \left\{2\left(1+\frac{c^2k^2}{|\omega_k|^2}\right)|\delta E_k^{(\pm)}|^2 + |\delta E_{kz}|^2\right\}, \\
&= -\frac{1}{4\pi L}\int_{\infty}^{\infty} dk e^{2\gamma_k t}\gamma_k \left\{2|\delta E_k^{(\pm)}|^2 + 2|\delta B_k^{(\pm)}|^2 + |\delta E_{kz}|^2\right\}, \\
&= -\frac{1}{8\pi L}\frac{\partial}{\partial t}\int_{-\infty}^{\infty} dk e^{2\gamma_k t}\left\{|\delta \boldsymbol{E}_k|^2 + |\delta \boldsymbol{B}_k|^2\right\}, \\
&= -\frac{\partial W_{EM}}{\partial t}.
\end{aligned}
\tag{1.4.54}
$$

where $|\delta \boldsymbol{E}_k| = 2|\delta E_k^{(\pm)}|^2 + |\delta E_{kz}|^2$ and $|\delta \boldsymbol{B}_k|^2 = 2\left|\delta B_k^{(\pm)}\right|^2$.

Indeed, kinetic energy temporal evolution correspond to the temporal change in the electromagnetic fields.

1.4.6 Plasma susceptibilities for a bi-Maxwellian velocity distribution

Let us consider the case in wich F_μ is a bi-Maxwellian for each $\mu-$species of the form

$$
F(v_\perp, v_\parallel, t) = \frac{1}{\pi^{3/2}u_\perp^2 u_\parallel^2}\exp\left[-\frac{v_\perp^2}{u_\perp^2} - \frac{v_\parallel^2}{u_\parallel}\right]. \tag{1.4.55}
$$

where $u_{\parallel\mu} = \sqrt{2k_B T_{\parallel\mu}/m_\mu}$ and $u_{\perp\mu} = \sqrt{2k_B T_{\perp\mu}/m_\mu}$ are the parallel and perpendicular thermal speeds with respect to the background magnetic field. Assuming that the distribution evolves keeping the form given.

Firstly, using the longitudinal susceptibility

$$
\chi_\mu^{zz} = \frac{\omega_{p\mu}^2}{2\omega}\int dv_\perp dv_\parallel \frac{v_\perp v_\parallel}{\omega - v_{\parallel k}}\frac{\partial F_\mu}{\partial v_\parallel} \tag{1.4.56}
$$

and replacing the Bi-Maxwellian distribution, now this expression yields

$$
\chi_\mu^{zz} = \frac{\omega_{p\mu}^2}{u_{\parallel\mu}^2 k^2}\frac{1}{2\pi}[1 + \xi Z(\xi_\mu)]. \tag{1.4.57}
$$

With that, replacing in the longitudinal dispersion relation, we get

$$1 + 2\sum_{\mu} \frac{\omega_{p\mu}^2}{u_{\parallel\mu}^2 k^2}[1 + \xi_\mu Z(\xi_\mu)] = 0. \tag{1.4.58}$$

Identically, the electromagnetic susceptibility is evaluated.

$$\begin{aligned}\chi_\mu^{(\pm)} &= \frac{\omega_{p\mu}^2}{4\omega^2}\int dv_\perp dv_\parallel \frac{v_\perp^2}{\omega - v_\parallel k \pm \Omega_\mu}\left[(\omega - \boldsymbol{v}\cdot\boldsymbol{k})\frac{\partial F_\mu}{\partial v_\perp} + v_\perp k \frac{\partial F_\mu}{\partial v_\parallel}\right], \\ &= \frac{\omega_{p\mu}^2}{4\pi\omega^2}[A_\mu + (\xi_\mu^0 + A_\mu \xi_\mu^\pm) Z(\xi_\mu^\pm)]. \end{aligned} \tag{1.4.59}$$

Therefore, the evaluated transverse susceptibility takes the form

$$1 - \frac{c^2k^2}{\omega^2} + \sum_\mu \frac{\omega_{p\mu}^2}{\omega^2}[A_\mu + (\xi_\mu^0 + A_\mu\xi_\mu^\pm)Z(\xi_\mu^\pm)] = 0. \tag{1.4.60}$$

Where it has been defined $t = v_\parallel/u_{\parallel\mu}$, $\xi_\mu = \omega/u_{\parallel\mu}k$, $R_\mu = u_{\perp\mu}^2/u_{\parallel\mu}^2$, $A_\mu = R_\mu - 1$ is the anisotropy and $Z(\xi)$ is the plasma dispersion function defined by Fried and Conte as

$$Z(\xi) = \frac{1}{\sqrt{\pi}}\int_{-\infty}^{\infty} dt \frac{e^{-t^2}}{t-\xi}. \tag{1.4.61}$$

More detailed calculations on the evaluated susceptibilities are developed in the subsection A2.1 and subsection A2.2.

1.4.7 Quasilinear equations

Considering the moments worked out previously for any distribution F_μ, now these are evaluated for a Bi-Maxwellian velocity distribution function with no drift evolving throughout time, i.e. in the plasma reference frame in absence of any shift in its normal modes whose dispersion relations where determined in the preceding section. In consequence,

$$\begin{aligned}\frac{\partial\langle\langle v_\parallel\rangle\rangle}{\partial t} = -\left(\frac{q_\mu}{m_\mu c}\right)^2 \frac{2i}{L}\int_{-\infty}^{\infty} dk \frac{e^{2\gamma_k t}}{k}\Bigg\{&\frac{c^2}{u_\parallel^2}[1 + \xi_\mu^0 Z(\xi_\mu^0)|\delta E_{kz}|^2 + \dots \\ &[A_\mu + (\xi_\mu^0 + A_\mu\xi^\mp)]Z(\xi_\mu^\mp)|\delta B_k^{(\pm)}|^2\Bigg\},\end{aligned} \tag{1.4.62}$$

$$\frac{\partial \langle\langle v_\parallel^2 \rangle\rangle}{\partial t} = -\left(\frac{q_\mu}{m_\mu c}\right)^2 \frac{4i}{L}\int_{-\infty}^{\infty} dk \frac{e^{2\gamma_k t}}{k^2}\left\{\omega_k \frac{c^2}{u_{\parallel\mu}^2}[1+\xi_\mu Z(\xi_\mu)]|\delta E_{kz}|^2 + \dots \right.$$
$$\left. \left(\omega_k \mp \Omega_\mu[A_\mu + (\xi_\mu^0 + A_\mu \xi_\mu^\mp)Z(\xi_\mu^\mp)] + \omega_k\right)|\delta B_k^{(\pm)}|^2\right\}, \tag{1.4.63}$$

$$\frac{\partial \langle\langle v_\perp^2 \rangle\rangle}{\partial t} = -\left(\frac{q_\mu}{m_\mu c}\right)^2 \frac{4i}{L}\int_{-\infty}^{\infty} dk \frac{e^{2\gamma t}}{k^2}\left\{(2i\gamma_k \mp \Omega_\mu)[A_\mu + (\xi_\mu^0 + A_\mu \xi_\mu^\mp)Z(\xi_\mu^\mp)] + \omega_k\right\}|\delta B_k^{(\pm)}|^2. \tag{1.4.64}$$

We have derived the relevant equations governing the evolution of the parallel and perpendicular second-order moments of a Bi-Maxwellian velocity distribution function. Already from Equation 1.4.62, which describes the evolution of the drift velocity, the connection between electromagnetic and electrostatic fluctuations becomes evident.

It is important to emphasize that quasilinear theory does not account for reshaping of the distribution function, nor does it include wave-wave or high-order wave-particle interactions, as demonstrated by E. Marsch [29]. Nevertheless, it does capture a mechanism for energy transfer across both electromagnetic and electrostatic wave-spectra–a process that has gained increasing attention [30, 31, 32] and has been supported by observational evidence [33, 34, 17]. Further discussion on this matter will be given in the chapter 3.
In this context, the quasilinear framework provides suitable first-order analytical approach to study the macroscopic behavior of the zeroth-order velocity distribution, as well as the growth and damping of fluctuations in the linear regime–a methodology that has been carefully developed and employed in previous works [1, 35, 36, 32, 37].

Thus, we have established the complete set of analytical developments—up to second-order perturbative expansion of the Vlasov equation—required to construct the quasilinear moment equations for a bi-Maxwellian velocity distribution function. These results lay the groundwork for their numerical resolution, which is the focus of the next chapter through the integration of equations Equation 1.4.63 and Equation 1.4.64. This numerical approach enables us to capture the time evolution of key macroscopic quantities, such as temperature anisotropy and wave energy density, under the influence of weakly nonlinear wave–particle interactions.

Chapter 2

Dispersion Relation Analysis and Adiabatic Evolution

From the previous chapter, we showed that linear perturbations to the Vlasov equation yield two independent dispersion relations under the assumption of a gyrotropic distribution and parallel propagation $k_\parallel$ with respect to the background magnetic field $\boldsymbol{B}_0$: a transverse electromagnetic mode and a longitudinal electrostatic mode.

These results underscore dispersion and anisotropy as two fundamental, yet not exclusive, properties of magnetized plasmas. Dispersion means that the phase velocity depends on the wave frequency, $v_\phi = \omega/k$, so we adopt the notation $\omega(k)$. Anisotropy arises from the directional dependence of plasma properties. In a magnetized system, particle motion becomes helical, coupling parallel and perpendicular velocities $(v_\parallel, v_\perp)$ to $\boldsymbol{B}_0$, leading to temperature anisotropy $T_\perp/T_\parallel$. This anisotropy also manifests in the plasma's electrical conductivity, described by the dielectric tensor $\check{\chi}_\mu$, which encodes the response to electromagnetic fields in different propagation directions. These two properties are deeply interconnected and central to understanding plasma behavior.

Although the title of this chapter broadly refers to the analysis of dispersion relations—each of which has been extensively studied individually in the literature—our primary focus lies on proton dynamics and their adiabatic evolution within a quasilinear framework. The chapter includes a discussion of the ion-acoustic mode, the electromagnetic component in isolation and its quasilinear evolution, followed by the combined interaction of both wave spectra, with emphasis on key parameters relevant to solar wind-type plasmas.

2.1 Electrostatic dispersion relation

Although magnetized plasmas generally support a broad spectrum of both electrostatic and electromagnetic modes, this work focuses on a specific subset: ion-acoustic waves propagating parallel to the background magnetic field, i.e., $\boldsymbol{k} \times \boldsymbol{B}_0 = \boldsymbol{0}$, and their relevance within this context.

From a fluid perspective, ion-acoustic waves correspond to compressive density perturbations–hence the term *acoustic*. These waves are supported by the interplay between the thermal motion of electrons and the inertia of ions, which in our case are proton, assuming a hydrogen plasma. The electrons provide thermal pressure that shapes the wave dynamics, while the ions contribute primarily through their mass. The dispersion relation in the fluid approximation is given by [27]:

$$\omega^2 = \frac{k^2 c_s^2}{1 + k^2 \lambda_{De}^2}. \tag{2.1.1}$$

Where $c_{s\mu}^2 = \gamma_e k_B T_\mu / m_\mu$ is the ion-acoustic sound speed, representing the proportionality between pressure and density variations in an ideal gas. The term λ_{De}^2 denotes the electron Debye length, k_B is the Boltzmann constant, and γ_e is a polytropic index for an ideal gas–it is the relation between pressure and density– in this case for electrons whose value is $\gamma_e = 3$ for 1D adiabatic compression.

Just as Alfvén waves can be accurately described within both magnetohydrodynamic (MHD) and kinetic frameworks (as will be discussed in the following section), ion-acoustic waves also possess an exact solution in the context of kinetic theory. In this framework, the electrostatic dispersion in a bi-Maxwellian proton VDF, relation takes the form:

$$1 + 2\sum_\mu \frac{\omega_{p\mu}^2}{u_{\parallel\mu}^2 k^2}[1 + \xi_\mu Z(\xi_\mu)] = 0, \tag{2.1.2}$$

where $\omega_{p\mu}^2$ is the plasma frequency, $u_{\parallel\mu}^2 = \sqrt{2k_B T_{\mu\parallel}/m_\mu}$ the parallel thermal speed with $\xi_\mu = \omega / k_\parallel u_\parallel$ is the resonance factor, and $Z(\xi)$ is the plasma dispersion function. This formulation captures the wave–particle interactions responsible for damping or instability, which are not accessible within fluid theory.

In the context of theoretical studies and space plasma physics, several works have traditionally neglected the role of ion acoustic modes, with a few notable exceptions [38, 39]. More recently, [17] analyzed data from the Parker Solar Probe [7], identifying heavily damped modes lacking correlated magnetic field signatures. These were interpreted as electrostatic longitudinal fluctuations capable of transferring energy to particles in the solar wind.

Since this research aims to understand the coupling between ion acoustic and electromagnetic waves, we introduce an additional source of free energy into the system. Specifically, a temperature difference between the species in a hydrogen plasma has been chosen as a representative case to explore various scenarios of interest. It is important to note that, in this section, we focus solely on a single source of free energy. However, in the analysis of the coupling between both modes, additional sources will be considered and discussed later.

From Figure 2.1.1, it is evident that for both $T_e = T_p$ and in extreme cases such as $T_e/T_p = 100$, the ion-acoustic wave is strongly damped, exhibiting an almost non-dispersive profile in the real frequency component. This suggests that such modes do not effectively propagate in the plasma. In contrast, the most pronounced wave activity occurs within the intermediate range $10 \leq T_e/T_p \leq 50$. Additionally, the system remains stable near $u_p k/\omega_{pp} \approx 0.4$, beyond which the wave amplitude diminishes, indicating a loss of coherence or the onset of damping. To numerically solve the dispersion relation, Equation 2.1.2, arising in the kinetic plasma theory it was employed the Muller [40] method.

These known results [41] highlight a critical parameter range in which ion-acoustic waves can persist with minimal damping and near-constant phase speed. Specifically, for temperature ratios in the range previously mentioned, where the system supports undamped electrostatic wave propagation. Beyond this threshold, kinetic damping mechanisms likely disrupt the wave's propagation.

While the present analysis does not yet incorporate nonlinear effects, mode coupling, or oblique propagation—where ion-acoustic wave effects become more pronounced [28]—it nonetheless establishes an important constraint for subsequent modeling efforts. The central result of this section is the identification of the electron-to-proton temperature ratio range within which ion-acoustic waves can play a dynamically significant role without being strongly suppressed by Landau damping. This bounded temperature regime will provide the basis for the forthcoming analysis of quasilinear coupling between ion-acoustic waves and Alfvén-cyclotron modes, which will be addressed in the next section.

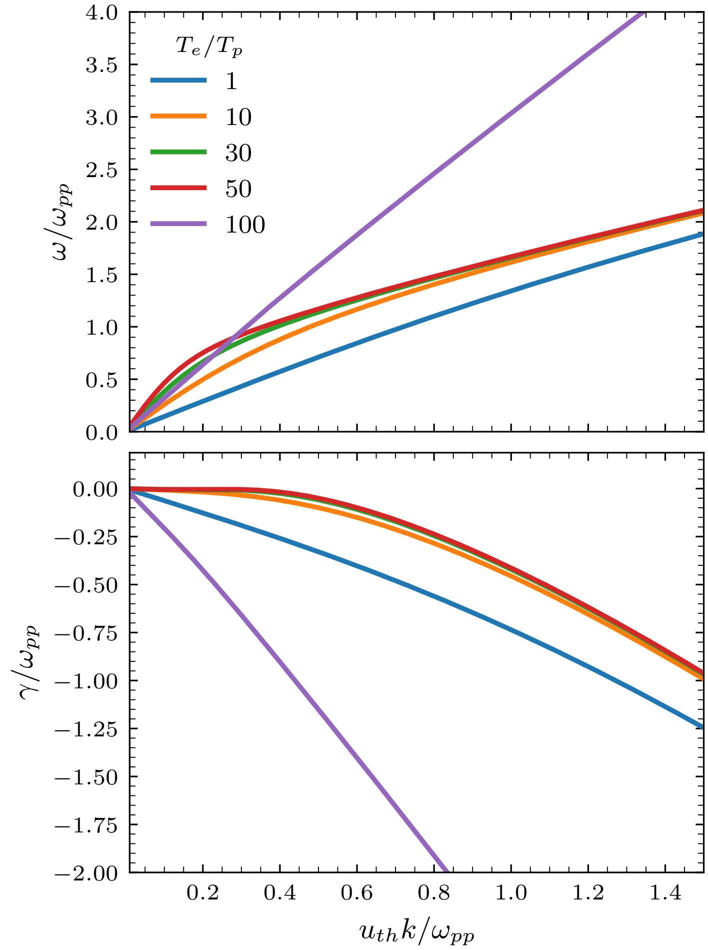

Figure 2.1.1: Solutions to the electrostatic kinetic dispersion relation shown in Equation Equation 2.1.2. We consider a plasma composed of Maxwellian protons and electrons, varying the temperature ratio T_e/T_p. The top panel displays the real part of the frequency ω/Ω_p, while the bottom panel shows the corresponding imaginary part γ/ω_{pp}. Note how the damping becomes significant for both low and high temperature ratios, with a clear window of reduced damping around intermediate values of T_e/T_p.

2.2 Electromagnetic dispersion relation

As previously mentioned, magnetized environments can support a wide variety of propagating wave modes, among which Magnetosonic and Alfvén waves are the most prominent and widely studied, both in the context of space plasmas [42, 43, 44] and in nuclear fusion reactors of the TOKAMAK type [45, 46, 47]. Both are well described within the framework of magnetohydrodynamics (MHD), which captures the collective behavior of plasma at macroscopic scales and short-wavelenght $v_A k/\Omega_p \ll 1$. These are also known as *hydromagnetic waves*, where an important assumptions is $\omega_r \ll \Omega_p$, meaning that these kind of waves have frequencies below the ion-cyclotron resonance. This section primarily focuses on the left-hand polarized Alfvén wave propagating parallel to the background magnetic field, i.e. $\boldsymbol{k} \times \boldsymbol{B}_0 = 0$.

Part of this section is also dedicated to reproducing the results obtained by Moya and Navarro [32], who conducted a linear study of the Alfvén wave dispersion relation and its quasilinear evolution under the influence of a constant-amplitude magnetic field spectrum.

According to MHD theory, Alfvén waves propagating parallel to a background magnetic field $\boldsymbol{B}_0$ are characterized by the simple dispersion relation:

$$\omega/k = v_A, \tag{2.2.1}$$

where $v_A \equiv B_0/(4\pi\rho_\mu)^{1/2}$ in CGS units, with B_0 as the background magnetic field amplitude and $\rho_\mu = n_\mu m_\mu$ representing the plasma mass density of the $\mu-$species. This concept was introduced by Alfvén [48], who demonstrated via Maxwell and hydrodynamics equations that such wave propagates through a plasma with a constant magnetic field at a characteristic phase velocity without plasma compression.

On the other hand, we have also seen that kinetic theory provides a more comprehensive description of wave modes, especially at small spatial scales or in weakly collisional plasma environments, where fluid models like MHD begin to lose validity. In this framework, we consider the dispersion relation for left-hand, circularly polarized electromagnetic waves propagating parallel to a uniform background magnetic field $\boldsymbol{B}_0$ in a bi-Maxwellian proton VDF. This relation, previously derived in section 1.4.6, takes the form:

$$\frac{\omega^2}{\Omega_p^2}\frac{v_A^2}{c^2} - \frac{v_A^2 k_\parallel^2}{\Omega_p^2} + \sum_\mu A_\mu + (\xi_\mu^0 + A_\mu \xi_\mu^-) Z(\xi_\mu^-) = 0, \tag{2.2.2}$$

where the index μ denotes the plasma species (e.g., electrons, protons, alphas, etc.)

The connection between equations (2.2.1) (the ideal MHD Alfvén wave) and (2.2.2) lies in the fact that, historically, the magnetohydrodynamic description has served as the foundational framework for understanding such waves. Alfvén first predicted their existence in 1942, proposing that these transverse, incompressible waves could propagate along magnetic field lines in a conducting fluid. He suggested that these waves might naturally occur in astrophysical environments such as the solar corona or the solar wind, where magnetic fields play a dominant role in plasma dynamics.

Kinetic theory extends this understanding by accounting for the resonant interactions between particles and waves, a feature absent in fluid models. In this context, the Alfvén wave is modified by ion-cyclotron effects, leading to what is often called the Alfvén-cyclotron wave. Despite the kinetic complexity, this mode retains the essential feature of propagating with a slope approximately given by the Alfvén speed v_A, thus bridging the gap between the fluid and kinetic pictures. See Figure 2.2.1.

Moreover, Alfvén waves have long been considered strong candidates in explaining coronal heating and solar wind acceleration, due to their ability to transport energy over large distances without immediate dissipation [49, 50, 51]. A thorough understanding of the kinetic behavior of these waves is therefore essential, either to resolve the solar heating problem or, at the very least, to advance our knowledge in this area.

2.2.1 Alfvén-Cyclotron Wave: Linear regime and Quasilinear evolution

In this section, we present a parametric study of the Alfvén-Cyclotron Wave (ACW), replicating and extending some of the results from Moya and Navarro [32] in the linear regime, as well as the quasilinear evolution of ACWs in the presence of an external guiding field. As mentioned in the introduction, temperature anisotropy serves as a free energy source in the system. By assuming a gyrotropic velocity distribution, perpendicular and parallel temperatures—associated with their respective velocity components—are treated as independent degrees of freedom. This follows directly from the invariance of the distribution function with respect to the pitch angle relative to the magnetic field direction.

Another key parameter in this analysis is the plasma beta, which in kinetic theory (expressed in CGS units) is defined as:

$$\beta_{\mu\|} = \frac{8\pi k_B n_\mu T_{\mu\|}}{B_0^2}, \tag{2.2.3}$$

where n_μ and $T_{\mu\|}$ are the number density and parallel temperature of the species μ, respectively.

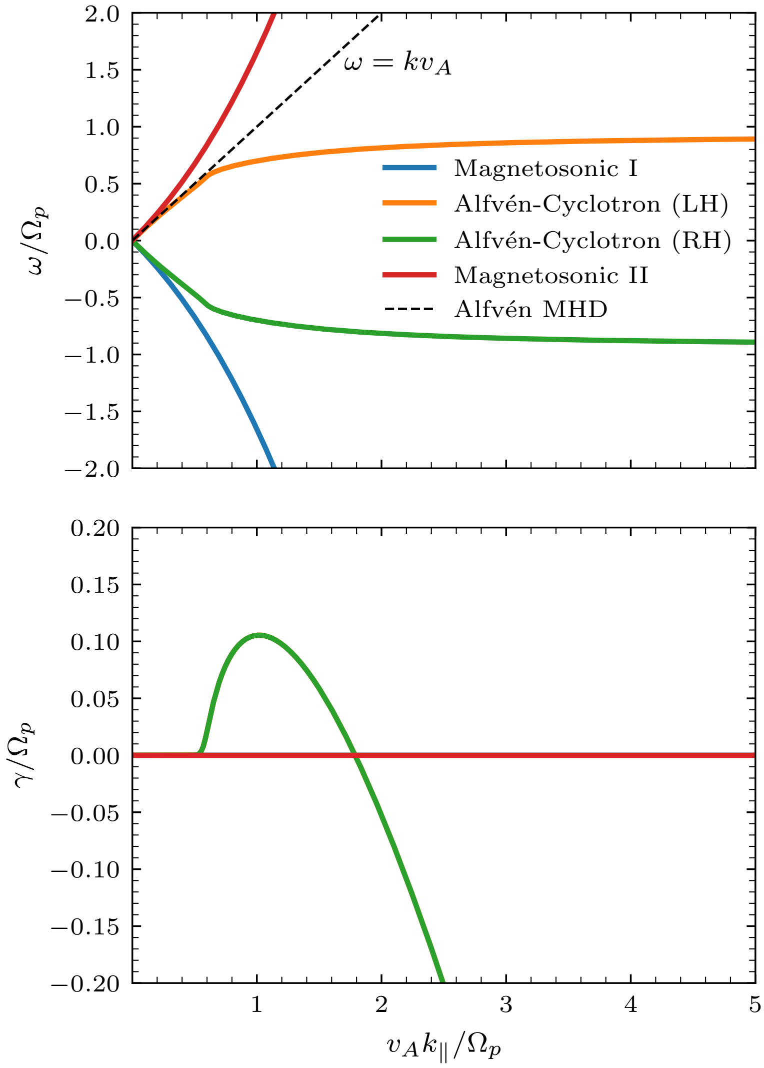

Figure 2.2.1: Solutions to the kinetic electromagnetic dispersion relation Equation 2.2.2. The top panel displays the real frequency ω/Ω_p for electromagnetic waves considering left-hand ($P = -1$) and right-hand ($P = +1$) polarization. For $P < 0$, we identify the magnetosonic I wave (blue) and the left-hand Alfvén–cyclotron wave (orange); for $P > 0$, we observe the right-hand Alfvén–cyclotron wave (green), the magnetosonic II wave (red), and the ideal MHD Alfvén wave (dashed). The bottom panel shows the corresponding damping/growth rates γ/Ω_p, where both Alfvén–Cyclotron branches exhibit the same damping profile, as do both magnetosonic branches. The plasma considered is kinetic for both protons and electrons, with a proton temperature anisotropy $T_\perp/T_\parallel = 5$, isotropic electrons, and a proton parallel beta $\beta_\parallel = 0.1$. The MHD Alfvén wave agrees with the kinetic modes at low wavenumbers.

In magnetized plasmas, particles follow cyclotron orbits due to the Lorentz force, and this expression quantifies the ratio between their parallel kinetic energy (numerator) and the magnetic confinement energy imposed by the background field (denominator). Hence, the parallel plasma beta serves as a measure of the relative importance of thermal pressure to magnetic pressure, and plays a fundamental role in determining wave stability and dispersion properties in collisionless plasmas.

Let us now consider a magnetized plasma composed of bi-Maxwellian protons and cold electrons. The kinetic dispersion relation for left-hand, circularly polarized waves propagating parallel to a uniform background magnetic field given by:

$$\frac{v_A^2 k_\parallel^2}{\Omega_p^2} = A + (A\xi^- + \xi)Z(\xi^-) - \frac{\omega_k}{\Omega_p}. \tag{2.2.4}$$

where $\omega_k = \omega_r + i\gamma$ is the complex frequency for a given wavenumber $k_\parallel$, $v_A = B_0/\sqrt{4\pi n_p m_p}$ is the Alfvén speed, with n_p and m_p the density and mass of protons, respectively; $\Omega_p = qB_0/m_p c$ is the proton gyrofrequency, with c the speed of light and q the proton charge,; $A = T_\perp/T_\parallel - 1$; $\xi_\mu = \omega/k_\parallel u_{\mu\parallel}$ and $\xi_\mu^- = (\omega/k_\parallel - \Omega_\mu)/k_\parallel u_{\parallel\mu}$ are resonance factors; $u_{\parallel\mu} = \sqrt{2k_B T_{\mu\parallel}/m_\mu}$ is the parallel thermal speed, with k_B the Boltzmann constant; and $Z(\xi)$ is the plasma dispersion function, which is calculated numerically with the Faddeeva function provided by SciPy. It also defined $\beta_{\parallel\mu} = u_{\parallel\mu}^2/v_A^2$ as de reduced beta parameter. All variables are written in CGS units. This expression is shown and worked in [52, 53, 54]. Further details of this derivation in section A3.

To numerically solve the dispersion relations arising in kinetic plasma theory, it was employed the Muller [40] method: a root-finding algorithm designed for complex-valued functions. This method is an iterative procedure that approximates the root of a function by fitting a parabola through three initial complex guesses and using the intersection of this parabola with the $x-$axis as the next estimate. Unlike the Newton-Raphson method, Muller's algorithm does not require explicit knowledge of the function's derivative, making it suitable for complex and computationally expensive dispersion relations. The method is robust and converges quickly in the vicinity of isolated roots, even in the presence of branch cuts or steep gradients in the complex plane. Here, it was applied the Muller method to find the complex frequencies ω_k satisfying the dispersion relation Equation 2.2.2, Equation 2.2.4, and Equation 2.1.2 for a given wavevector $k_\parallel$, thereby enabling the identification of unstable modes and the characterization of wave growth rates in various plasma configurations.

Figure 2.2.2 presents an initial parameter scan over temperature anisotropies and $\beta_\parallel$ values. On the left panel, we observe the formation of the resonance for $v_A k_\parallel/\Omega_p > 1$ in the real frequency ω/Ω_p, and how increasing the anisotropy progressively drives the onset of the instability. On the right panel, for $\beta_\parallel < 1$, the real part of the frequency appears to asymptotically approach

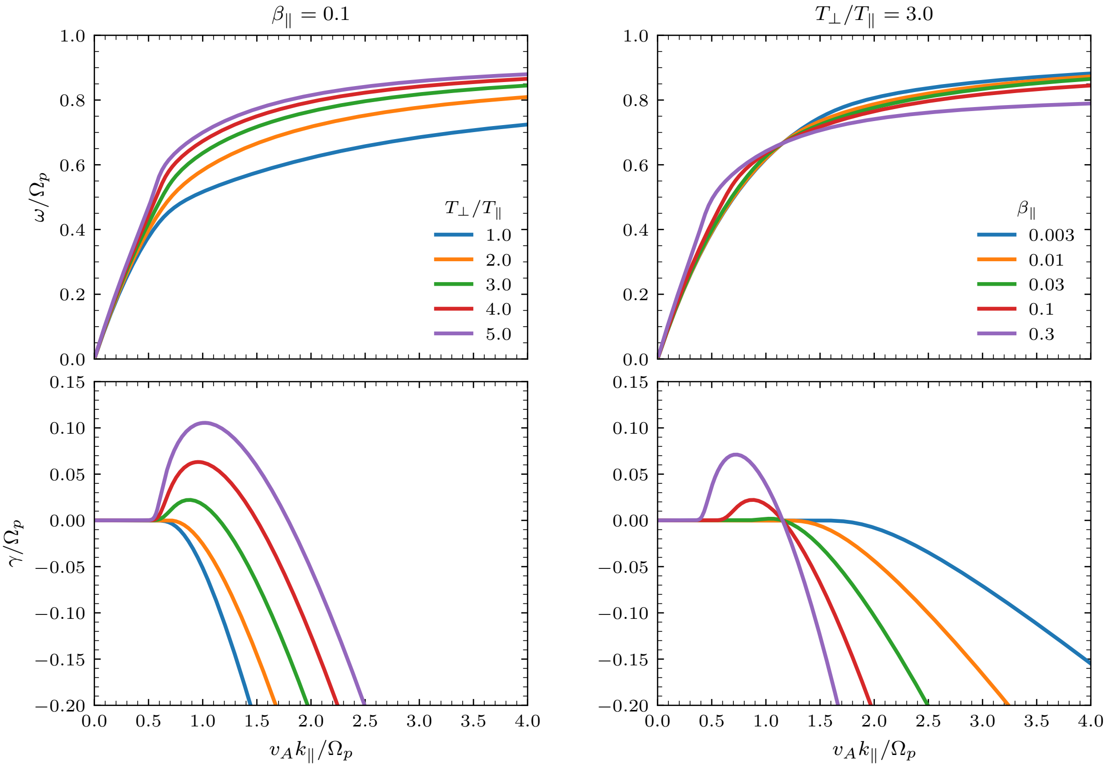

Figure 2.2.2: Frequency and growth/damping rates of Alfvén-cyclotron waves as a function of $k_\parallel$, computed using Equation 2.2.4. The left panel (top: real part, bottom: imaginary part) displays the wave profile for $\beta_\parallel = 0.1$. The right panel shows the corresponding results for a fixed temperature anisotropy of $T_\perp/T_\parallel = 3.0$.

$\omega = \Omega_p$, as established in [32]. Meanwhile, the corresponding imaginary part shows that for these low beta values, the system remains marginally stable—i.e., $\gamma/\Omega_p = 0$—and does not reach the threshold for instability excitation.

Last observation is crucial, as it serves as the foundation for numerically determining the instability contours shown in Figure 2.2.3. We extended the parameter space over $(\beta_\parallel, T_\perp/T_\parallel)$ and computed the maximum values of γ/Ω_p. Plasma configurations with $\gamma/\Omega_p \leq 10^{-3}$ are considered stable in this analysis.

The quasilinear moments theory (QLT) assumes that the macroscopic parameters evolves adiabatically, that is to say that $\omega_k = \omega_k(t)$ solves dispersion relations and at all times. The evolution of the perpendicular and parallel thermal speed for protons are worked here are also given by [1, 32, 37]:

$$\frac{\partial u_{p\parallel}^2}{\partial t} = \mathrm{Im}\,\frac{q^2}{m_p^2}\frac{8}{L}\int_{-\infty}^{\infty} dk_\parallel e^{2\gamma t}\frac{|\delta B_k|^2}{c^2k^2}\left[(\omega_k - \Omega_p)\left(\frac{v_A^2 k_\parallel^2}{\Omega_p^2} + \frac{\omega_k}{\Omega_p}\right) + \omega_k\right]. \tag{2.2.5}$$

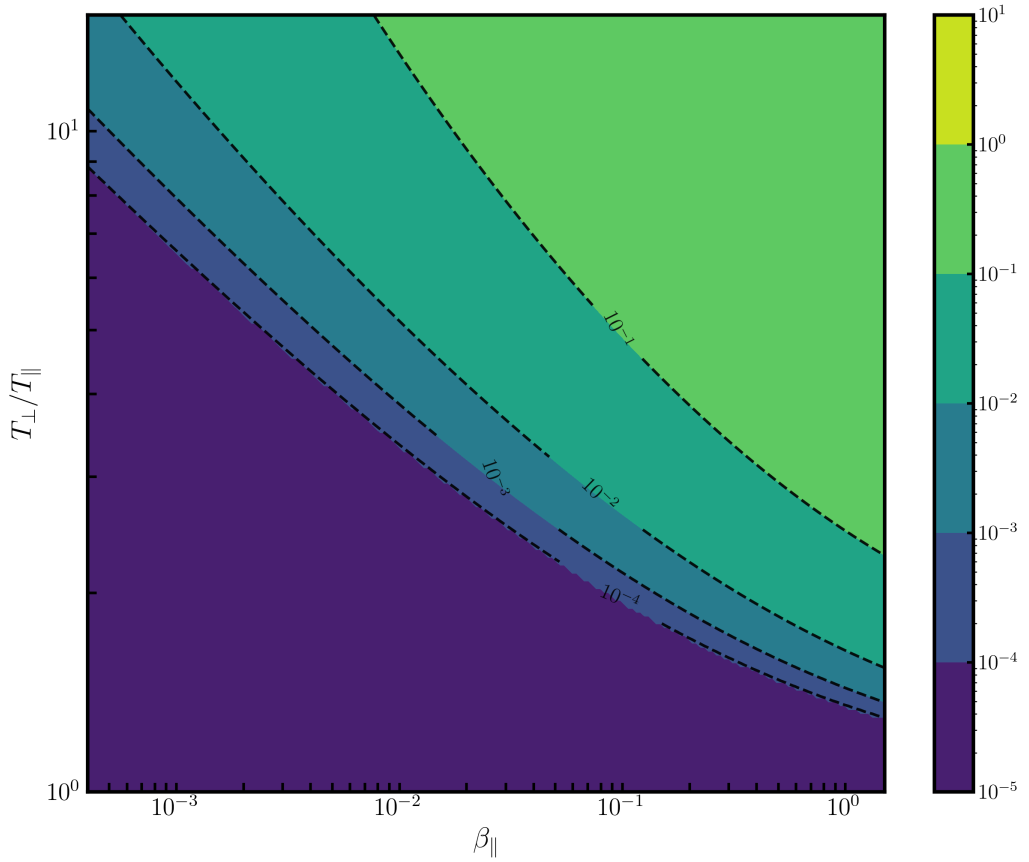

Figure 2.2.3: Instability thresholds for the Alfvén-Cyclotron wave (ACWs) numerically calculated from Equation 2.2.2, spanning the range $2 \times 10^{-2} \leq \beta_\parallel \leq 15$ and $1 \leq T_\perp/T_\parallel \leq 15$. Color bar represents the maximum growth rate $\gamma_{\max}$. A configuration will be considered stable when $\gamma/\Omega_p \leq 10^{-3}$.

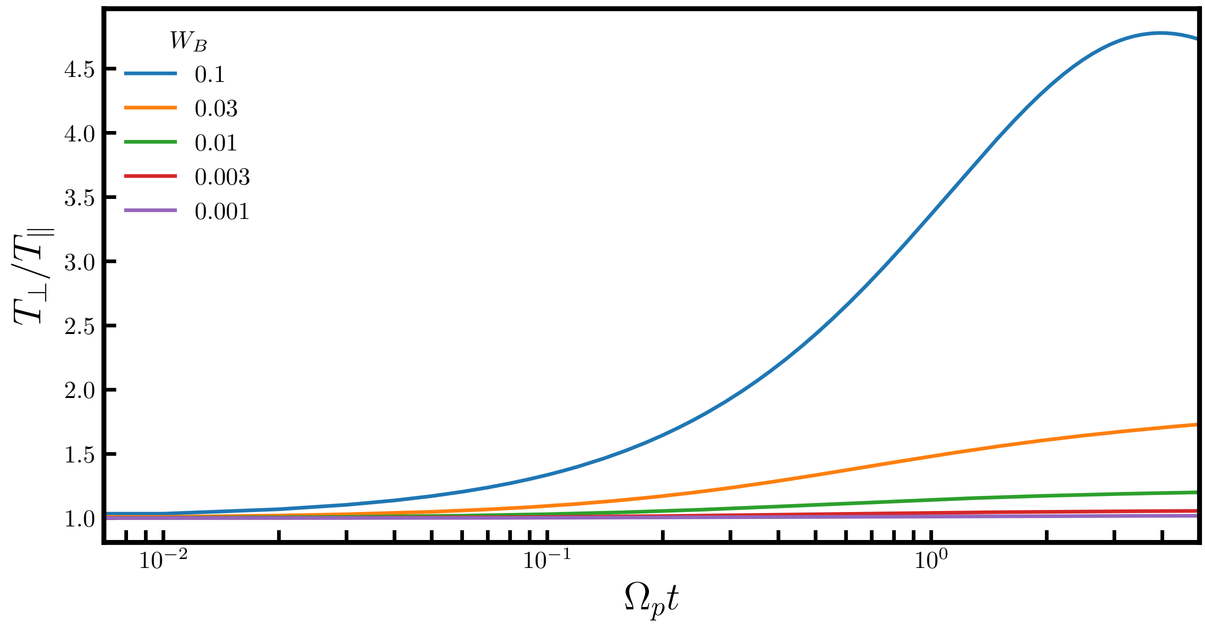

Figure 2.2.4: Quasilinear evolution of proton temperature anisotropy. Initial conditions for this case are $T_\perp(0)/T_\parallel(0) = 1$, and $\beta_\parallel(0) = 0.1$ for different values of initial magnetic energy (uniform spectrum) $W_B(0) = 0.1$ (blue), $W_B(0) = 0.03$ (orange), $W_B(0) = 0.01$ (green), $W_B(0) = 0.003$ (red), and $W_B(0) = 0.001$ (purple).

$$\frac{\partial u_{p\perp}^2}{\partial t} = -\,\mathrm{Im}\,\frac{4}{L}\frac{q^2}{m_p^2}\int_{-\infty}^{\infty} dk_\parallel e^{2\gamma t}\frac{|\delta B_k|^2}{c^2k^2}\left[(2i\gamma - \Omega_p)\left(\frac{v_A^2k_\parallel^2}{\Omega_p^2} + \frac{\omega_k}{\Omega_p}\right) + \omega_k\right]. \tag{2.2.6}$$

This is where the replication phase begins more deeply: the initial magnetic spectrum is taken to be uniform, such that $|B_k(0)|^2 = A$, with the wavenumber range defined by $10^{-3} < v_A k_\parallel/\Omega_p < 8$. Under these conditions, quasilinear simulations are carried out by evolving the corresponding partial differential equations in time. The evolution of key macroscopic plasma parameters can be seen in Figure 2.2.4, Figure 2.2.5, and Figure 2.2.6.

The three figures referenced above are intended solely to illustrate the system's saturation state for different values of magnetic energy W_B and do not represent full simulations. Nevertheless, it is worth noting that initially stable configurations—such as those discussed in Figure 2.2.2—can evolve into unstable states when energy is injected into the system. Eventually, these configurations settle into a new equilibrium, adjusting themselves within the boundaries of the instability thresholds. This self-regulation mechanism is particularly relevant for understanding energy redistribution and stability in space plasmas, such as the solar wind, where continuous energy input and nonlinear wave–particle interactions play a key role in shaping plasma dynamics.

Further discussion and results of this simulations can be found in [32] where these were performed

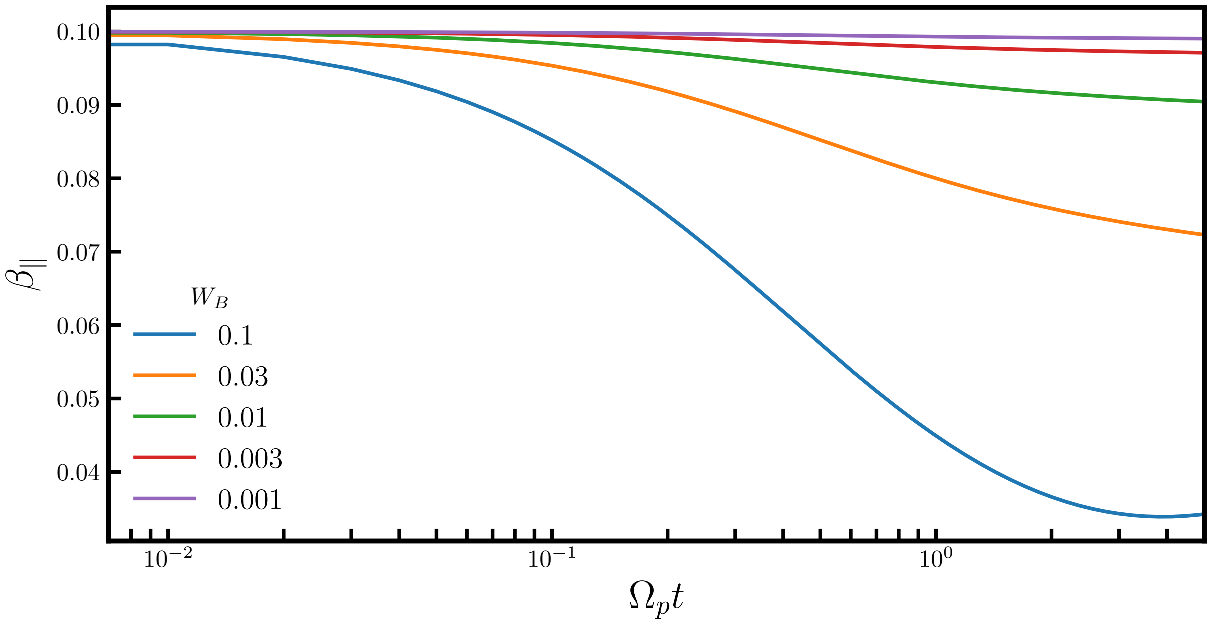

Figure 2.2.5: Quasilinear evolution of the proton parallel beta parameter. Initial conditions for this case are $T_\perp(0)/T_\parallel(0) = 1$, and $\beta_\parallel(0) = 0.1$ for different values of initial magnetic energy (uniform spectrum) $W_B(0) = 0.1$ (blue), $W_B(0) = 0.03$ (orange), $W_B(0) = 0.01$ (green), $W_B(0) = 0.003$ (red), and $W_B(0) = 0.001$ (purple).

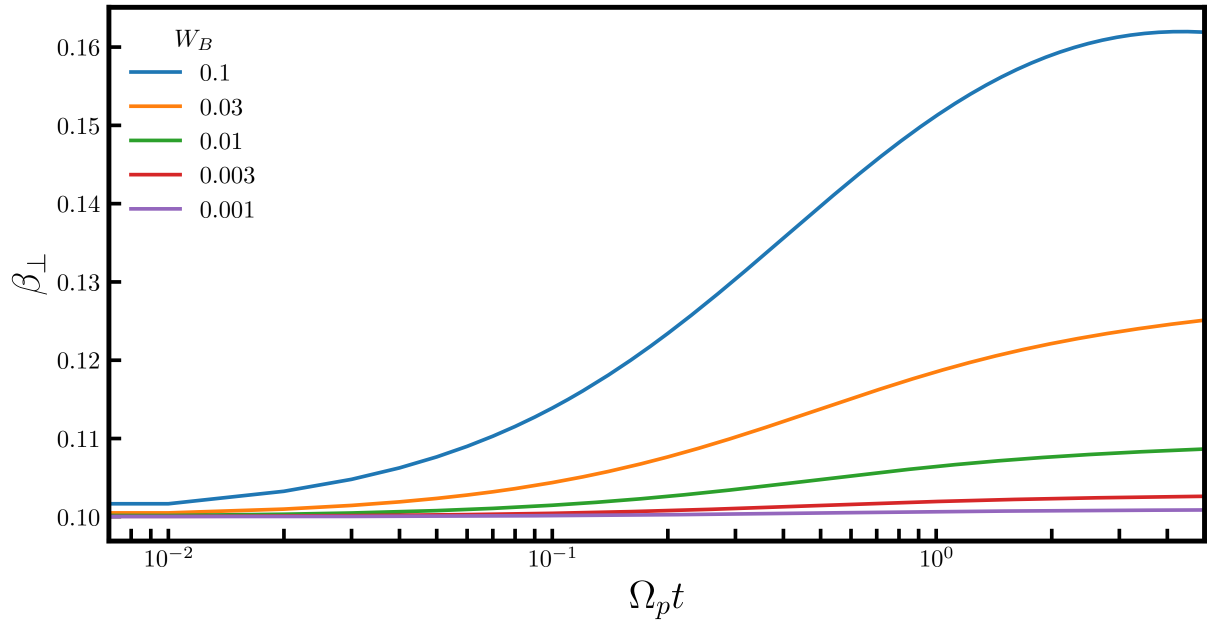

Figure 2.2.6: Quasilinear evolution of the proton perpendicular beta parameter . Initial conditions for this case are $T_\perp(0)/T_\parallel(0) = 1$, and $\beta_\parallel(0) = 0.1$ for different values of initial magnetic energy (uniform spectrum) $W_B(0) = 0.1$ (blue), $W_B(0) = 0.03$ (orange), $W_B(0) = 0.01$ (green), $W_B(0) = 0.003$ (red), and $W_B(0) = 0.001$ (purple).

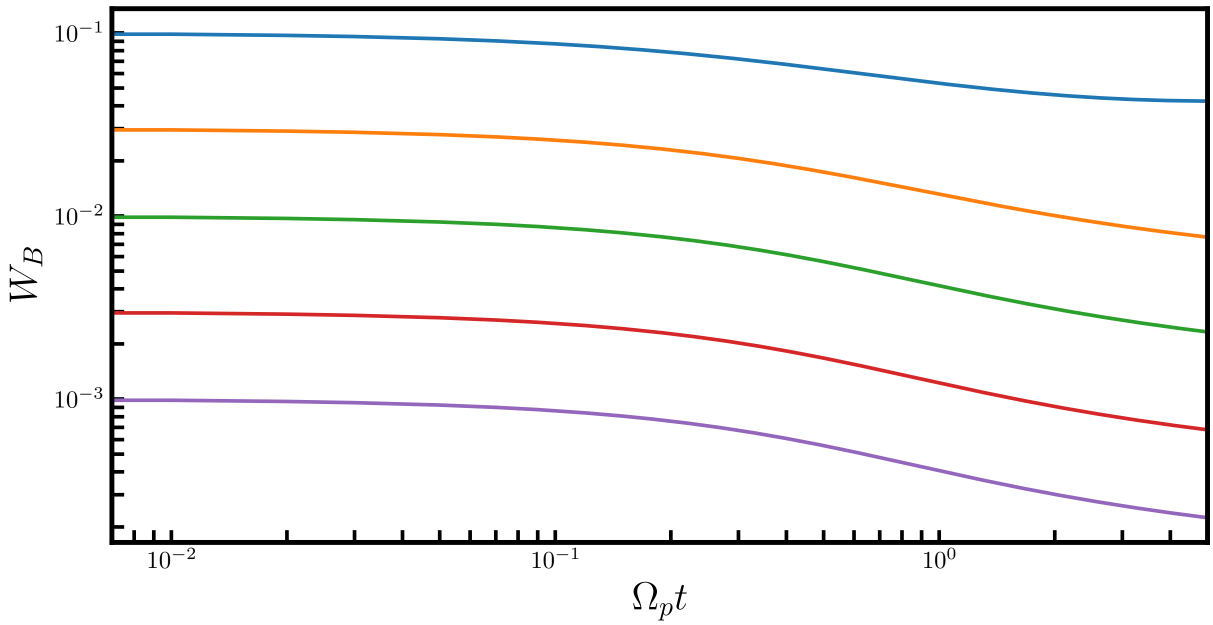

Figure 2.2.7: Quasilinear evolution of the magnetic energy. Initial conditions for this are in agreement with previous figures: $T_\perp(0)/T_\parallel(0) = 1$, and $\beta_\parallel(0) = 0.1$ for different values of initial magnetic energy (uniform spectrum) $W_B(0) = 0.1$ (blue), $W_B(0) = 0.03$ (orange), $W_B(0) = 0.01$ (green), $W_B(0) = 0.003$ (red), and $W_B(0) = 0.001$ (purple).

for larger times.

Figure 2.2.8 summarizes the entire parameter space described above, displaying the time evolution of $\beta_\parallel$, $T_\perp/T_\parallel$, and W_B. A series of quasilinear simulations were performed using initial conditions evenly spaced in logarithmic scale over the range $0.003 \leq \beta_\parallel \leq 0.3$ and $1 \leq T_\perp/T_\parallel \leq 5$, indicated by white circles. Each simulation begins with a uniform magnetic wave spectrum characterized by an initial energy of $W_B(0) = 0.01$. The colored trajectories in the diagram represent the temporal evolution of the system in this parameter space, with color encoding the instantaneous magnetic energy W_B. The colored circles denote the system's final state at $\Omega_p t = 150$, well after reaching a quasi-stationary regime, using the same color scale to indicate W_B. This figure encapsulates how different initial conditions evolve under quasilinear dynamics, highlighting the system's tendency to relax toward the marginal stability boundaries previously discussed.

In this way, we have partial but successfully reproduced the key results relevant to the objectives of this investigation. This serves as a necessary foundation for addressing the main goal of the study: to examine the effects of introducing a second propagation mode—namely, ion-acoustic waves—into the system, simultaneously coupled with the effects of an external electric field. As a preparatory step toward this objective, we will first present the global behavior of the system under the condition of a minimized magnetic field amplitude. This configuration enables us to isolate the influence of electrostatic interactions and provides a controlled baseline for

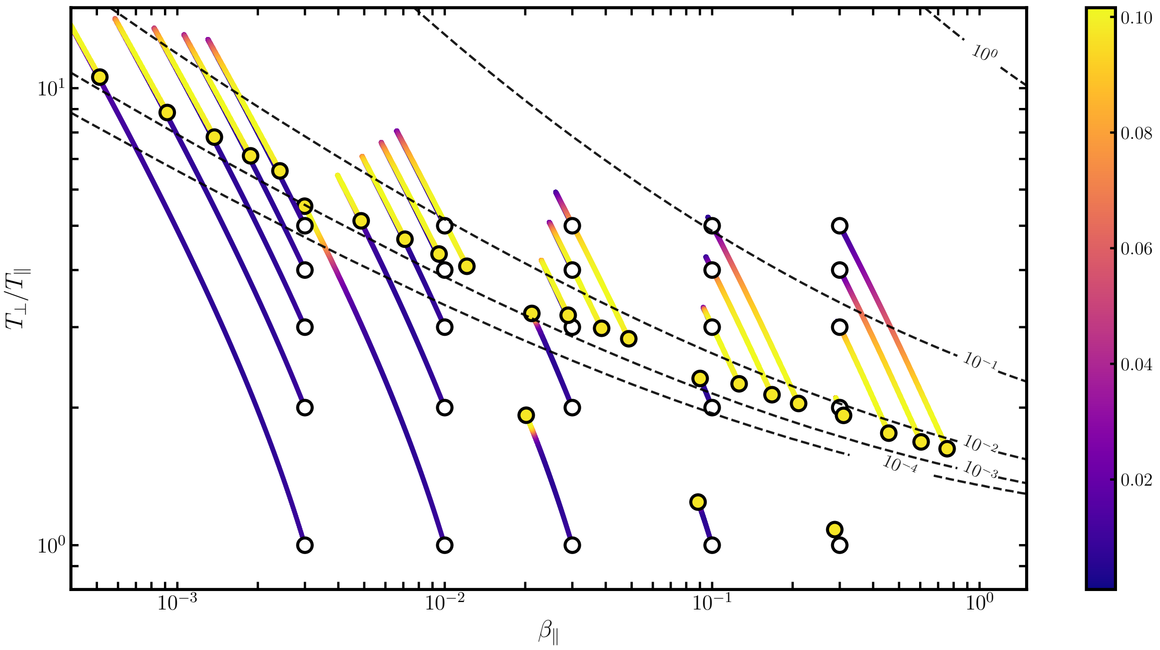

Figure 2.2.8: Quasilinear evolution of the proton $\beta_{p\parallel}$ and anisotropy $T_\perp/T_\parallel$. Initial conditions (white circles) were chosen evenly spaced in the range $0.03 \leq \beta_\parallel \leq 0.3$ and $1 \leq T_\perp/T_\parallel \leq 5$, with an uniform magnetic wave spectrum power of $W_B(0) = 0.01$ for all cases. The colorbar represent the instantaneous value of $W_B(t)$. Dashed lines are contours of the proton-cyclotron instability with maximum growth-rates $\gamma/\Omega_p = 10^{-4}$ to 10^0, as calculated from the dispersion relation Equation 2.2.2. Colorized circles correspond to the stationary (final) state of the plasma simulations.

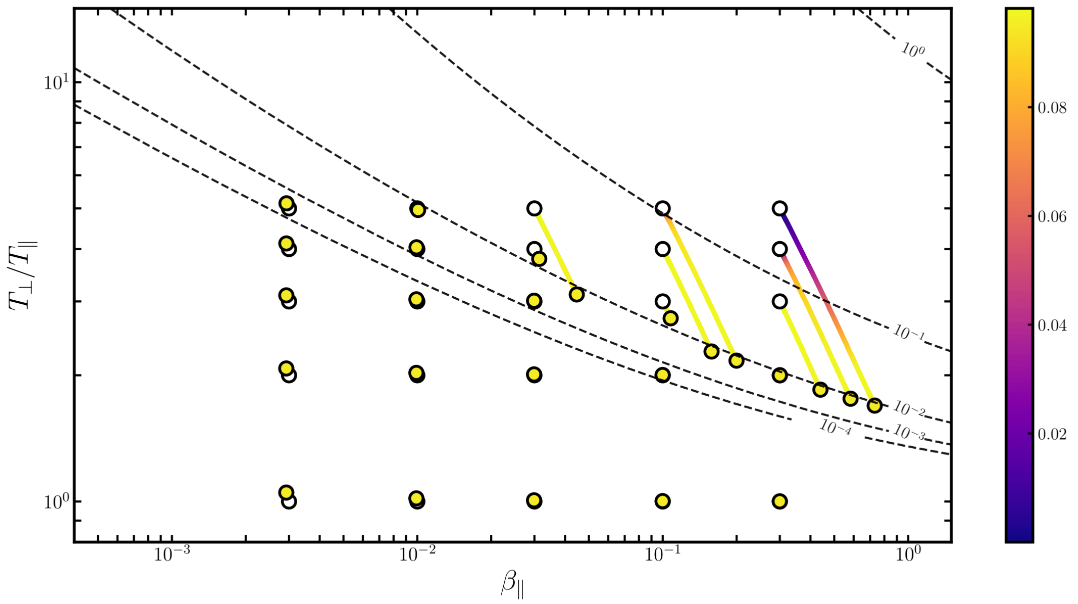

Figure 2.2.9: Quasilinear evolution of the proton $\beta_{p\parallel}$ and anisotropy $T_\perp/T_\parallel$. Initial conditions (white circles) were chosen evenly spaced in the range $0.03 \leq \beta_\parallel \leq 3$ and $1 \leq T_\perp/T_\parallel \leq 5$, with an uniform magnetic wave spectrum power of $W_B(0) = 10^{-5}$ for all cases. The colorbar represent the instantaneous value of $W_B(t)$. Dashed lines are contours of the proton-cyclotron instability with maximum growth-rates $\gamma/\Omega_p = 10^{-4}$ to 10^0, as calculated from the dispersion relation Equation 2.2.2. Colorized circles correspond to the stationary (final) state of the plasma simulations.

evaluating the combined effects in the subsequent section.

In Figure 2.2.9, we present simulations performed across various configurations within the parameter space $0.03 \leq \beta_\parallel \leq 3$ and $1 \leq T_\perp/T_\parallel \leq 5$. These runs were carried out with the sole purpose of assessing the influence of a weak background magnetic field. In this case, the magnetic field spectral amplitude was set to $W_B(0) = 10^{-5}$ for a uniform spectrum. We observe that for all configurations deemed stable—specifically, those lying below the instability contour defined by $\gamma/\Omega_p = 10^{-4}$—the background magnetic field fails to inject significant energy into the system, and as a result, these configurations exhibit no temporal evolution. In contrast, configurations that are initially unstable, such as those with temperature anisotropy $T_\perp/T_\parallel = 5$ and $\beta_\parallel = 3$, 1, or 0.1, undergo damping and evolve toward the corresponding instability contours.

The white markers in the figure indicate the initial conditions at $t = 0$, while the yellow markers denote the (quasi-)stationary final states reached after the nonlinear evolution. In this way, we have effectively isolated the influence of the background magnetic field by minimizing its amplitude. This allows us to fix this parameter in subsequent simulations, ensuring that its contribution remains negligible. As a result, the following parametric study can more clearly assess the role of additional wave modes—such as the electrostatic ion-acoustic waves—on the nonlinear evolution and anisotropy regulation of the plasma system.

2.3 Ion-Acoustic Wave Effects on Proton Transverse Heating†

This section is dedicated to analyzing the influence and interplay between the two wave spectra previously introduced, both assuming parallel propagation to a uniform background magnetic field $\boldsymbol{B}_0$. As demonstrated in the previous chapter, particularly in Equation 1.4.25, the two corresponding solutions to the dielectric tensor $\check{\chi}_\mu$ are linearly independent. However, at second-order perturbation in the Vlasov equation, these modes become entangled through the slow-time evolution of the distribution function F_μ. To further motivate this coupling, we emphasize the inherent scale separation between the two spectra. In magnetized plasma environments–such as the solar wind or the Earth's magnetosphere–this distinction is supported by both theoretical models and spacecraft observations. Ion-Acoustic Waves (IAWs), associated with the ion plasma frequency, have been theorized in the heating of solar wind [55] and observed in the kilohertz range in regions such as the plasma sheet by missions like Solar Orbiter [56, 34]. On the other hand, progress has been made through missions that are believed to have already detected Alfvén waves, notably by spacecraft such as ACE [57], and more recently, the Parker Solar Probe [58, 7, 59].

This disparity is also reflected in our model through the adoption of two distinct normalization schemes. For IAWs, we have used $\bar{\omega} = \omega/\omega_{pp}$ and $\bar{k} = u_{p\parallel}k_\parallel/\omega_{pp}$, while for ACWs we define $\tilde{\omega} = \omega/\Omega_p$ and $\tilde{k} = v_A k_\parallel/\Omega_p$. This approach not only highlights the physical separation between the two branches but also allows us to treat their mutual interaction within a coherent multiscale framework.

In absence of a second hotter species, either electrons or protons, ion acoustic waves are heavily damped and since we are looking for an instability it is necessary look for a resonant condition thus it could compete with the EMIC instability. The interplay between electrostatic and electromagnetic spectral modes–and their combined role in plasma energization–remains insufficiently understood, partly due to the large separation of scales involved. A comprehensive understanding of these problems requires deeper investigation into the mechanism of energy transfer in space and space-like plasmas, as a gas generally needs some form of irreversible dissipation and inter-species energy exchange to approach thermodynamic equilibrium. This aspect gains particular relevance when different free energy reservoirs operate simultaneously within the same plasma whose in situ measurements reveal local non-thermal equilibrium.

Here, we investigate the nonlinear interaction between ion-acoustic electrostatic fluctuations and

†A substantial portion of this section is based on the manuscript *"Proton-Acoustic Wave Effects on the Relaxation of Proton Transverse Heating in Magnetized Plasmas"* by M. A. Quijada, P. S. Moya, and R. E. Navarro, submitted to the special issue *Focus on Plasma Physics in Latin America*, Physica Scripta.

Alfvén-Cyclotron instabilities contributes to energy redistribution and temperature anisotropy relaxation in solar wind-type plasmas. Using quasilinear moment theory [1, 2] and quasilinear numerical simulations, we systematically study how these coupled wave modes drive the slow-in-time, collective evolution of the VDF and affect the relaxation of macroscopic plasma properties.

Figure 2.3.1 displays the Alfvén-Cyclotron Wave (ACW, red) and the Ion-Acoustic Wave (IAW, blue), with the real part of the frequency shown in the upper panel and the imaginary part in the lower panel, for four different electron-to-proton temperature ratios T_e/T_p. Both wave branches are presented using the same normalization for wavenumber and frequency. On the one hand, the real part of the ACW remains essentially unchanged across all cases, while the IAW exhibits a slight variation in its dispersive behavior. The most significant changes, however, are observed in the damping/growth rates: as the temperature ratio increases, the ACW gradually loses its instability, while the IAW progressively recovers, giving rise to a stable region around $v_A k_\parallel/\Omega_p \approx 1$.

On the other hand, since $\beta_{e\parallel}/\beta_{p\parallel} = u_{\text{the}}^2/u_{\text{thp}}^2$, Figure 2.3.2 displays four cases corresponding to different values of the electron parallel beta parameter $\beta_{e\parallel}$. The solutions for the Alfvén-Cyclotron Wave (ACW, in red) and Ion-Acoustic Wave (IAW, in blue) are shown, with the real part of the frequency in the top panel and the imaginary part in the bottom panel. In this case, we observe that both wave branches share a low wavenumber region, $v_A k_\parallel/\Omega_p < 1$, which may suggest a possible coupling or resonance for $\beta_{e\parallel}$ values between 1.0 and 1.5. As $\beta_{e\parallel}$ increases further, the branches become more clearly separated; however, in panel **(d)**, the instability appears to recover in the IAW branch.

2.3.1 Effect of a Uniform Electric Background Spectrum on the Quasilinear Evolution

As the previous case studied before, we consider a magnetized plasma composed of bi-Maxwellian protons and electrons VDFs, with the difference that the latter act as an isotropic thermal bath of constant temperature T_e. The kinetic dispersion relations of left-handed circularly polarized waves and longitudinal waves propagating along a background magnetic field $\boldsymbol{B}_0$, respectively, are simultaneously solved and given in Equation 2.2.2 and Equation 2.1.2 which are solved at all times. Thus, the evolution of the perpendicular and parallel thermal speed for protons, due our chosen normalization, are given by

$$\frac{\partial \tilde{u}_\perp^2}{\partial \tilde{t}} = i\frac{v_A}{c}\int d\tilde{k}_\parallel e^{2\tilde{\gamma}\tilde{t}v_A/c}\frac{|\tilde{B}_k|^2}{\tilde{k}_\parallel^2}[(2i\tilde{\gamma}-1)\tilde{\chi}_p^- + \tilde{\omega}], \tag{2.3.1}$$

$$\frac{\partial \tilde{u}_\parallel^2}{\partial \tilde{t}} = -2i\frac{v_A}{c}\int d\tilde{k}_\parallel e^{2\tilde{\gamma}\tilde{t}v_A/c}\frac{|\tilde{B}_k|^2}{\tilde{k}_\parallel^2}[(\tilde{\omega}+1)\tilde{\chi}_p^- + \tilde{\omega}] - 2i\frac{c}{v_A}\frac{1}{\sqrt{\beta_{\parallel p}}}\int d\bar{k}_\parallel e^{2\bar{\gamma}\bar{t}}\bar{\chi}_p^{zz}\frac{|\bar{E}_k|^2}{\bar{k}_\parallel^2}\bar{\omega}. \tag{2.3.2}$$

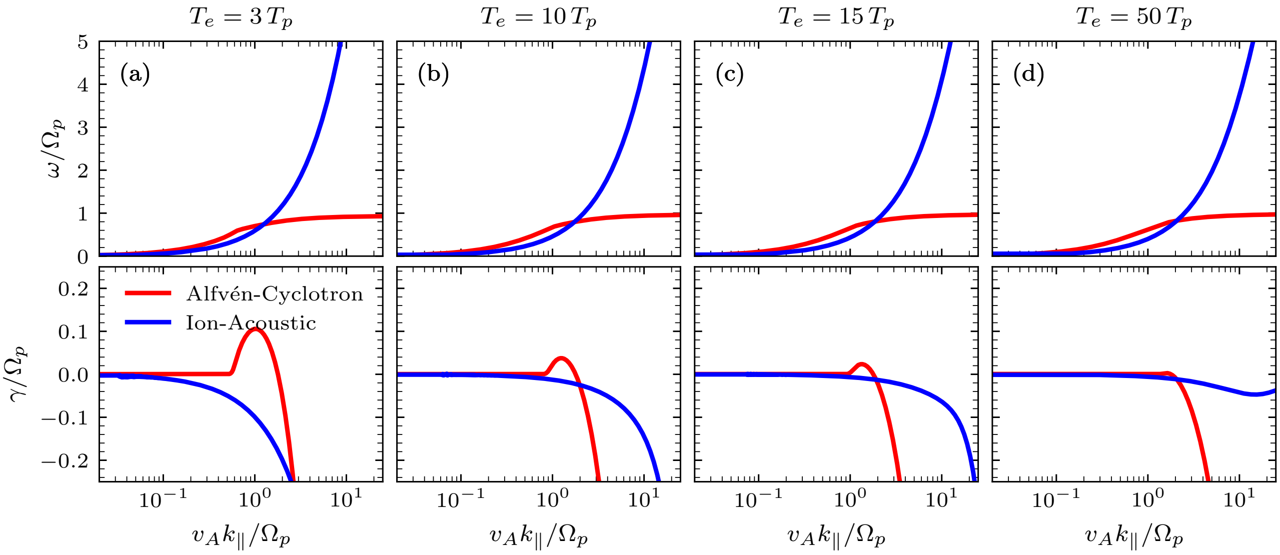

Figure 2.3.1: (Top) Frequency and (bottom) growth/damping rate of the Alfvén-Cyclotron (red) and Ion-Acoustic (blue) wave modes as a function of wavenumber $v_A k_\parallel/\Omega_p$, as calculated from the dispersion relation Equation 2.2.2 and Equation 2.1.2. Wavenumbers are shown in logarithmic scale. Each column show results from different temperature ratios T_e/T_p, with fixed $T_{p\perp}/T_{p\parallel} = 5$ and $\beta_{e\parallel} = 0.3$. This is equivalent to vary the proton beta as $\beta_{p\parallel} = 0.1$, 0.03, 0.02, 0.006, respectively.

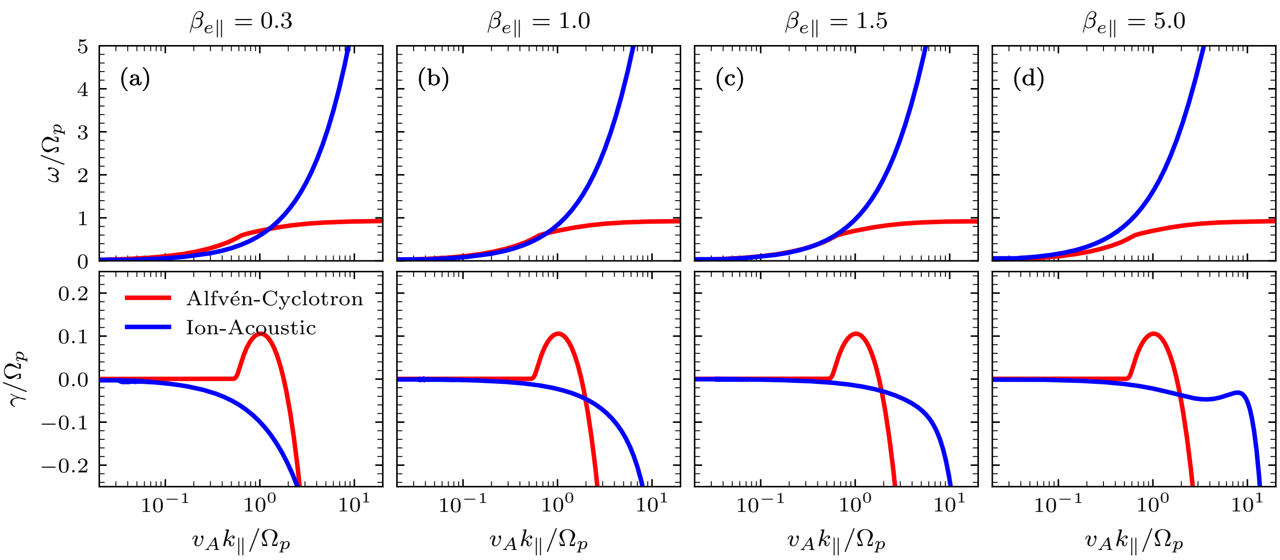

Figure 2.3.2: Frequency and growth/damping rate of Alfvén-Cyclotron (red) and Ion-Acoustic (blue) waves as a function of a single wavenumber $k_\parallel$, as calculated from the dispersion relation Equation 2.2.2 and Equation 2.2.2 with the temperature ratio T_e/T_p fixed for each case. $T_{p\perp}/T_{p\parallel} = 5$ and $\beta_{p\parallel} = 0.1$.

Since we have adopted $\tilde{u}_{\perp,\parallel} = u_{\perp,\parallel}/v_A$, for the thermal speeds and $\tilde{t} = t\omega_{pp}$ for time, the field amplitudes are similarly normalized as $|\tilde{B}_k|^2 = 4|B_k|^2 q_p^2/m_p^2 v_A L\Omega_p c^2, |\bar{E}_k|^2 = 4|E_k|^2 q_p^2/m_p^2 v_A L\Omega_p c^2$. It is worth noting the following identity, which connects the two characteristics frequencies in our model: $\Omega_p/\omega_{pp} \equiv v_A/c$. This equivalence not only ensures the consistency of the electromagnetic and electrostatic normalizations, but also plays a crucial role in the temporal evolution of equations Equation 2.3.1 and Equation 2.3.2. As seen in in both expressions, this ratio sets the characteristics rate in the exponential damping or growth of the spectral fields, directly influencing the dynamics of the system. Therefore, we can establish the relevant physical parameters of the system: $\beta_{p,e\parallel}$, proton anisotropy $T_{p\perp}/T_{p\parallel}$, field amplitudes$|B_k|^2$, $|E_k|^2$, and the speed ratio v_A/c. We have chosen $\tilde{t} = t\omega_{pp}$, in contrast with similar works [35, 32, 37], where $\tilde{t} = t\Omega_p$.

Thus, the quasilinear equations are presented as follows,

$$\frac{\partial u_{\perp p}^2}{\partial t} = -\mathrm{Im}\frac{4}{L}\frac{q^2}{m_p^2}\int_{-\infty}^{\infty} dk_\parallel \frac{|B_k|^2}{c^2k^2} e^{2\gamma_k t}\left[(2i\gamma_k - \Omega_p)\chi_p^- + \omega_k\right], \tag{2.3.3}$$

$$\frac{\partial u_{\parallel p}^2}{\partial t} = \mathrm{Im}\frac{8}{L}\frac{q^2}{m_p^2}\int_{-\infty}^{\infty} dk_\parallel e^{2\gamma_k t}\left\{\left[(\omega_k - \Omega_p)\chi_p^- + \omega_k\right]\frac{|B_k|^2}{c^2k^2} + \chi_p^{zz}\frac{|E_{kz}|^2}{u_\parallel^2 k^2}\omega_k\right\}. \tag{2.3.4}$$

To solve numerically the system of differential equations given by Equation 2.3.3 and Equation 2.3.4, we use a trapezoidal method provided by NumPy library. For academic purposes, we considered two uniform background spectra for $|B_k|^2$ and $|E_k|^2$ to illustrate the effects that different configurations can produce on the quasilinear evolution of the macroscopic parameters of the plasma, that is to say, uniform noise $|B_k(0)|^2 = A$ and $|E_k(0)|^2 = B$. Where either of these amplitudes is adjusted on the initial total magnetic $W_B(0)$ or electric energy $W_E(0)$, with both integrals calculated in the range $10^{-3} < v_A k_\parallel/\Omega_p < 12$ and $10^{-3} < u_\parallel k_\parallel/\omega_{pp} < 2$, respectively.

2.3.2 Numerical Results

Figure 2.3.3 presents a parameter scan considering three different constant electric field amplitudes, while all other relevant physical parameters are held fixed. In the first row, showing the time evolution of the initial temperature anisotropy $T_{p\perp}(0)/T_{p\parallel}(0) = 5$, we observe that only for $|E_k|^2(0) = 10^{-4}$ the effect is significant, leading to a noticeable increase in perpendicular proton temperature. The remaining two amplitudes show minimal impact, with the anisotropy steadily decaying by $\omega_{pp}t = 100$.

Similarly, for the temperature ratio profile, we selected $T_e/T_p = 30$, and the behavior mirrors that of the proton anisotropy evolution. Notably, the most pronounced effects are observed in the decay of the electrostatic spectrum $|E_k|^2$ and in the evolution of the magnetic energy W_B.

Regarding the former, although the spectral energy drops sharply during the first few plasma periods, the cases with $|E_k|^2(0) = 10^{-5}$ and $|E_k|^2(0) = 10^{-6}$ begin from nearly negligible levels.

As for the magnetic energy, the bottom row of Figure 2.3.3 suggests a possible inverse correlation: as the electrostatic spectrum diminishes, magnetic energy appears to recover or grow, hinting at an energy exchange mechanism between the electric and magnetic fluctuations.

Having presented the electric field spectra, we now aim to analyze the evolution of field intensity over time. We observe that the shape of the electric field spectrum remains essentially unchanged throughout the simulation, with only its initial amplitude varying. In contrast, the magnetic field spectrum W_B exhibits a different behavior: it initially decreases and then recovers around $\omega_{pp}t \approx 100$.

As shown in Figure 2.3.4, the electric field energy remains concentrated at wavenumbers satisfying $u_{p\parallel}k_\parallel/\omega_{pp} < 1$ throughout the simulation. This supports the interpretation that the instability remains marginal, consistent with our earlier findings in Figure 2.1.1.

Regarding the magnetic field, whose spectral intensity is also linked to the instability of Alfvén-cyclotron waves (ACWs), we find that the instability remains marginal up to $v_A k_\parallel/\Omega_p \approx 1$. It becomes clearly excited within the range $1 \lesssim v_A k_\parallel/\Omega_p \lesssim 1.5$, and subsequently damps for higher wavenumbers.

The next case study focuses on the variation of temperatures between plasma species. As previously discussed in the section on ion-acoustic waves (IAWs), the temperature ratio range of interest is $10 \leq T_e/T_p \leq 50$. In the first row of Figure 2.3.5, we observe that increasing the ratio up to $T_e/T_p = 50$ leads to a more constrained anisotropy, in contrast to the case with $T_e/T_p = 20$. Regarding the temporal evolution of this parameter, all profiles exhibit a similar behavior. A comparable trend is found for the electric field energy W_E and its associated spectrum, as well as for the magnetic field energy W_B.

In light of these observations, we have also decided to study the evolution and intensity of the corresponding spectra over time. In Figure 2.3.6, we analyze how the intensity of each field evolves as a function of the electron-to-proton temperature ratio. For the magnetic field, we observe the same behavior described previously in Figure 2.3.4, particularly regarding the wavenumber range where the instability develops $v_A k_\parallel/\Omega_p \approx 1$. However, the electric field spectrum shows a distinct behavior: as the temperature ratio increases, the electric field appears to inject energy into regions where the instability is otherwise decaying. This suggests that the upper bound of the temperature ratio marks the threshold at which the instability becomes marginal.

A third parameter sweep is presented in Figure 2.3.7, where we analyze the quasilinear evolution of the plasma for different values of the proton parallel beta, $\beta_{p\parallel}$. For the case $\beta_{p\parallel} = 0.10$, we observe that an initially high anisotropy continues to increase, a behavior not seen in the

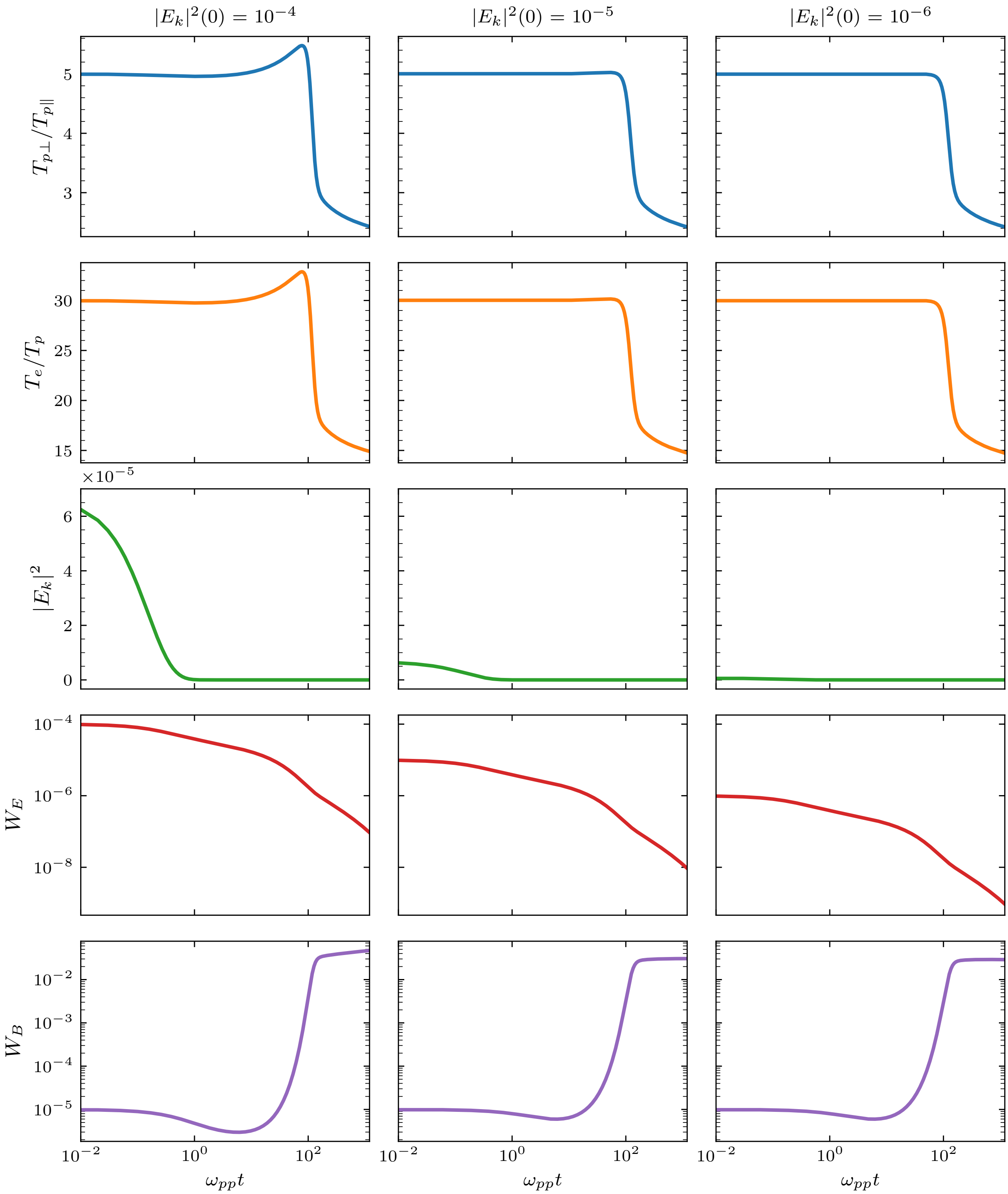

Figure 2.3.3: Quasilinear evolution under the influence of an electrostatic spectrum with constant amplitude $|E_k|^2(0) = 10^{-4}$, $|E_k|^2(0) = 10^{-5}$, and $|E_k|^2(0) = 10^{-6}$ for each column. The fixed parameters are $T_{p\perp}(0)/T_{p\parallel}(0) = 5$, $\beta_{p\parallel} = 0.1$, and $T_e/T_p = 30$. The initial values for electric and magnetic field energy are $W_E(0) = 10^{-4}$ and $W_B(0) = 10^{-5}$ in logarithmic scale.

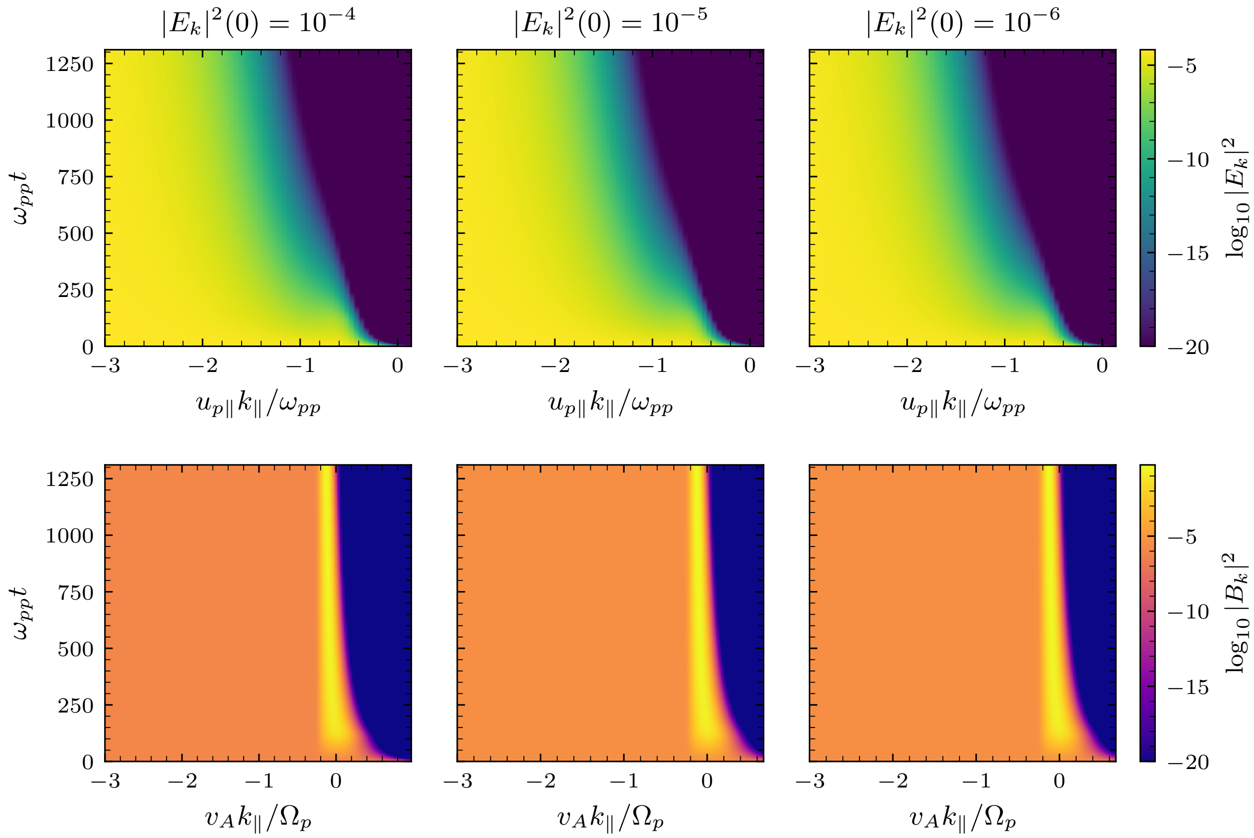

Figure 2.3.4: Time evolution of the electric (top row) and magnetic (bottom row) field power spectra for different initial electric field amplitudes, with the magnetic spectrum corresponding to a fixed value $|B_k|^2(0) = 10^{-5}$. Both spectra are shown as functions of their respective normalized wavenumbers on a logarithmic scale: $u_p k_\parallel/\omega_{pp}$ for the electric field and $v_A k_\parallel/\Omega_p$ for the magnetic field. Color bar indicates the logarithmic intensity of the fields over time. All other simulation parameters are consistent with those in Figure 2.3.3.

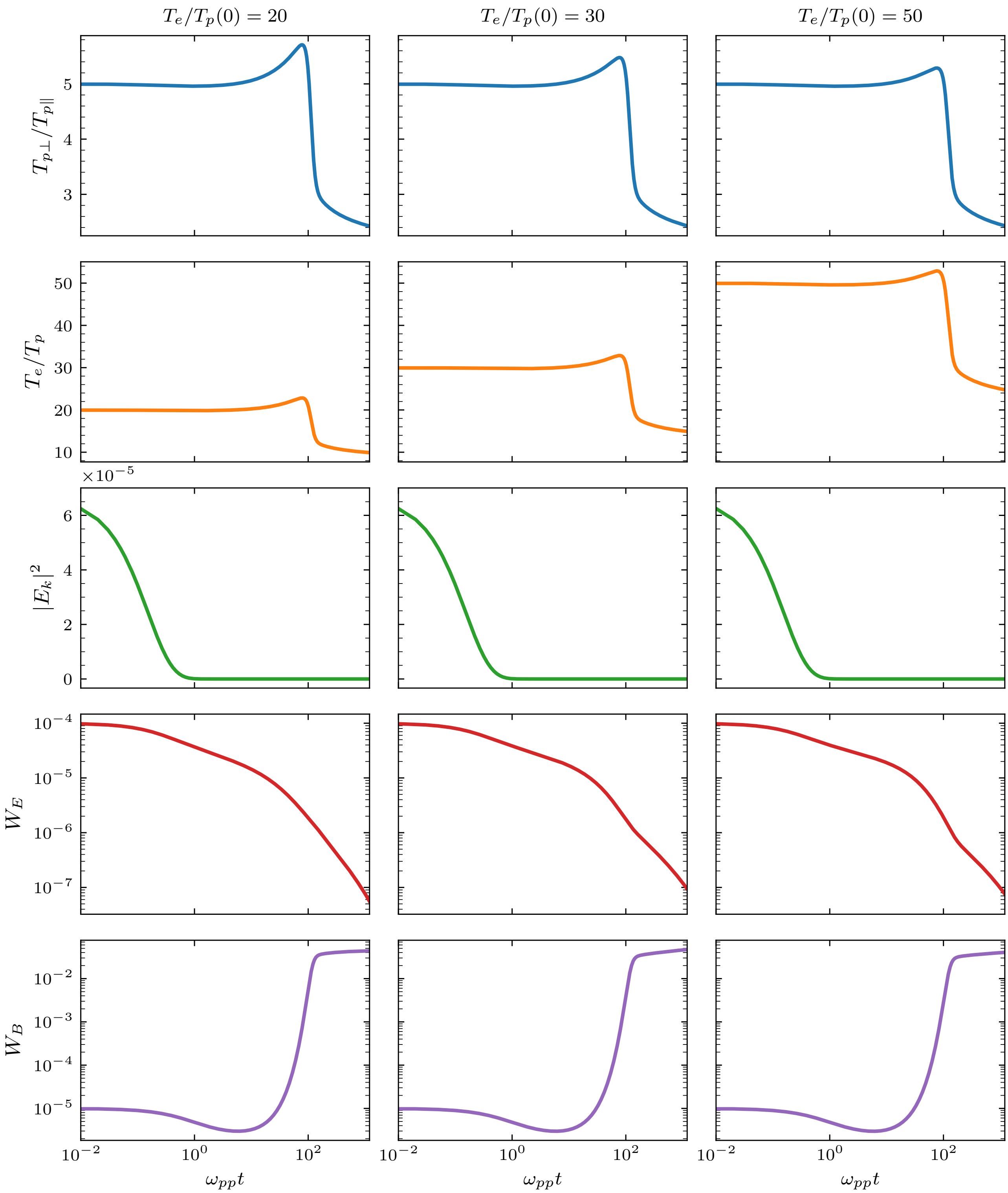

Figure 2.3.5: Quasilinear evolution for different temperatures ratios $T_e/T_p = 20$, $T_e/T_p = 30$, and $T_e/T_p = 50$ for each column. The fixed parameters are $T_{p\perp}(0)/T_{p\parallel}(0) = 5$, $|E_k|^2(0) = 10^{-4}$, $\beta_{p\parallel} = 0.1$, and $T_e/T_p = 30$. The initial values for electric and magnetic field energy are $W_E(0) = 10^{-4}$ and $W_B(0) = 10^{-5}$ in logarithmic scale.

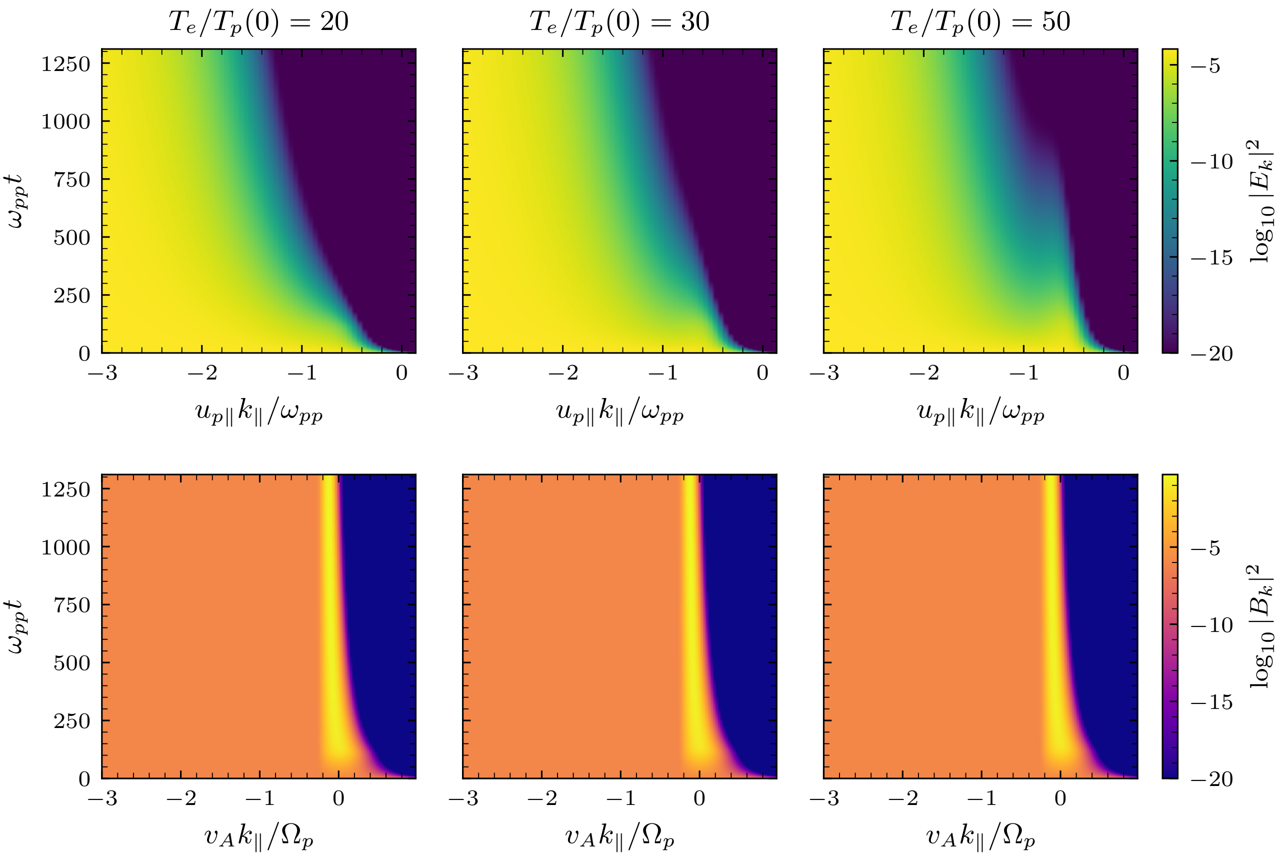

Figure 2.3.6: Time evolution of the electric (top row) and magnetic (bottom row) field power spectra as functions of their respective normalized wavenumbers, both shown on a logarithmic scale: $u_p k_\| / \omega_{pp}$ for the electric field and $v_A k_\| / \Omega_p$ for the magnetic field. Each column corresponds to a different electron-to-proton temperature ratio T_e/T_p, as defined in Figure 2.3.5. All cases assume $|E_k|^2(0) = 10^{-4}$ for the electric field and $|B_k|^2(0) = 10^{-5}$ for the magnetic field. The color bar represents the logarithmic field intensity over time.

other two cases. The corresponding temperature evolution follows a similar trend. Changes in the initial electric spectral energy, $|E_k|^2(0)$, appear to be minor across all cases; however, the magnetic energy evolution shows more significant variation. In particular, the increase in W_B is most prominent for $\beta_{p\parallel} = 1.00$.

Following the previous analysis, we also examined the temporal evolution of the field intensities. Figure 2.3.8 shows that the electric field energy remains concentrated at low wavenumbers, specifically in the regime $u_{p\parallel}k_\parallel/\omega_{pp} \ll 1$, and similarly for the magnetic field. However, the magnetic energy initially peaks around $v_A k_\parallel/\Omega_p = 1$ and progressively shifts toward lower values of $v_A k_\parallel/\Omega_p$ as the system evolves. This behavior is particularly evident for larger proton beta values, such as $\beta_{p\parallel} = 1.00$, where the instability becomes more prominent at smaller wavenumbers.

Figure 2.3.9 presents 40 simulations performed in the $(\beta_\parallel, T_\perp/T_\parallel)$ parameter space for two electron-to-proton temperature ratios: $T_e/T_p = 10$ (upper panel) and $T_e/T_p = 50$ (lower panel). The goal is to compare the effects of this temperature ratio on the quasilinear evolution of the system. These two cases represent the extremes of the previously defined range.

We observe that, for configurations with $T_\perp/T_\parallel \geq 2$ and $\beta_{p\parallel} \geq 0.3$—i.e., initially unstable conditions—trajectories tend to evolve toward the contours of constant growth rate γ/Ω_p. It is important to note that each instability contour was computed using the corresponding temperature ratio, since $\beta_{e\parallel}/\beta_{p\parallel} = u_{\mathrm{the}}^2/u_{\mathrm{thp}}^2$. This highlights from the outset the non-unique correspondence among parameters due to their interdependence.

Significant changes are observed for $\beta_{p\parallel} \leq 0.1$ and across their corresponding columns of anisotropies. We infer that, in regimes where the plasma tends to behave more like a fluid, electrostatic fluctuations become stronger under these conditions, and in turn, contribute to transverse particle heating, eventually bringing the system close to the EMIC (Electromagnetic Ion Cyclotron) marginal stability contours.

This chapter presented a brief study of Ion-Acoustic Waves (IAWs) and how the temperature ratio between species in a hydrogen plasma leads to a stable branch at low wavenumbers. This feature proves useful for coupling with the Alfvén-Cyclotron Wave (ACW) spectrum through a quasilinear framework. The second section focused on the replication of known linear results for ACWs and the adiabatic evolution of proton anisotropy under the influence of a uniform magnetic field, including a discussion on the effects of reducing this background field. Finally, a third section—an extension of the work submitted to *Focus on Plasma Physics in Latin America* (Physica Scripta)—addressed the combined interaction of both wave spectra. A parametric study was carried out exploring key physical parameters such as $\beta_{p\parallel}$, proton temperature anisotropy $T_{p\perp}/T_{p\parallel}$, field amplitudes $|B_k|^2$, $|E_k|^2$, and the electron-to-proton temperature ratio T_e/T_p.

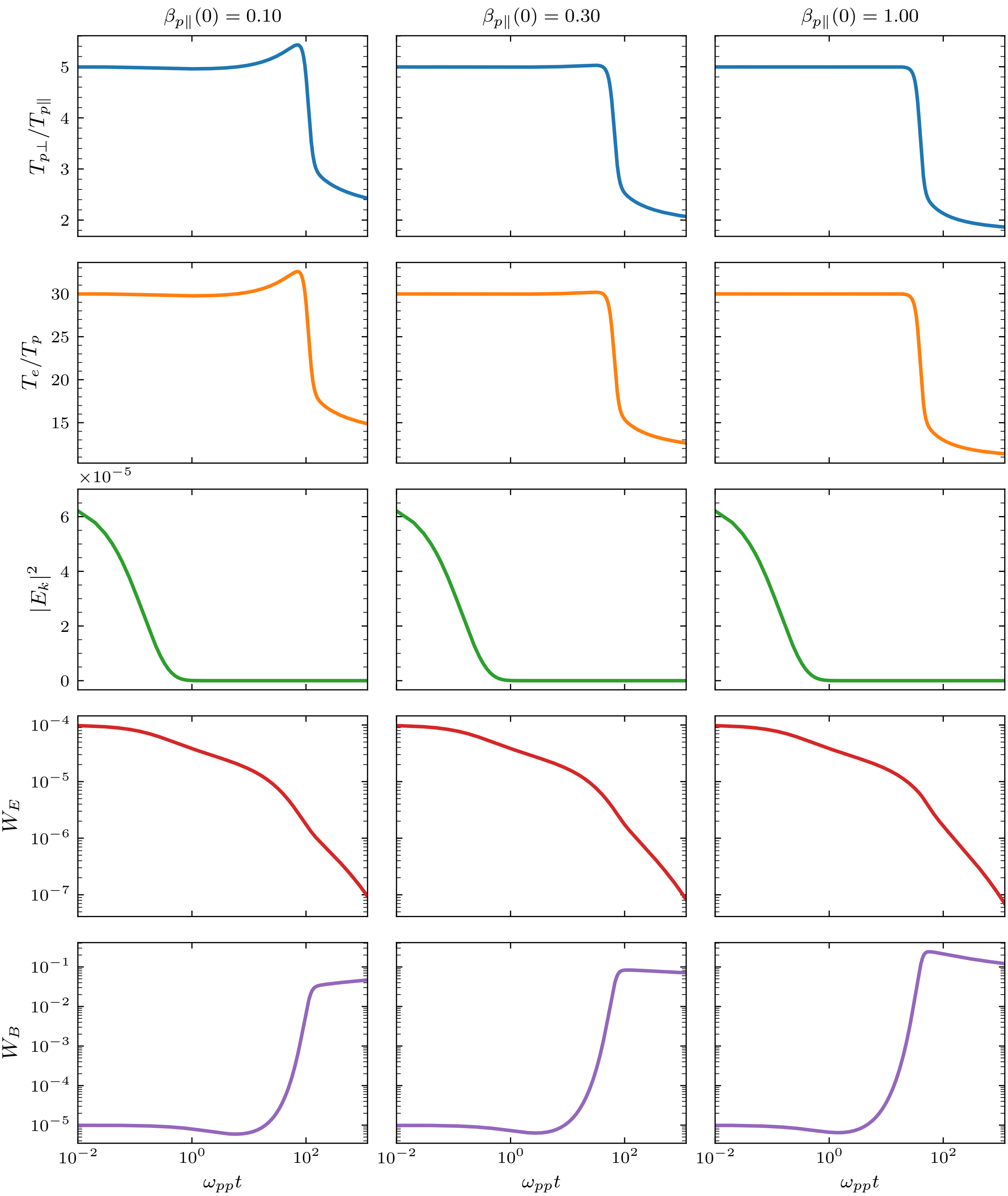

Figure 2.3.7: Quasilinear evolution for different proton beta parameters $\beta_{p\parallel} = 0.1$ for each column. The fixed parameters are $T_{p\perp}(0)/T_{p\parallel}(0) = 5$, $T_e/T_p = 30$, $|E_k|^2(0) = 10^{-4}$, and $T_e/T_p = 30$. The initial values for electric and magnetic field energy are $W_E(0) = 10^{-4}$ and $W_B(0) = 10^{-5}$ in logarithmic scale.

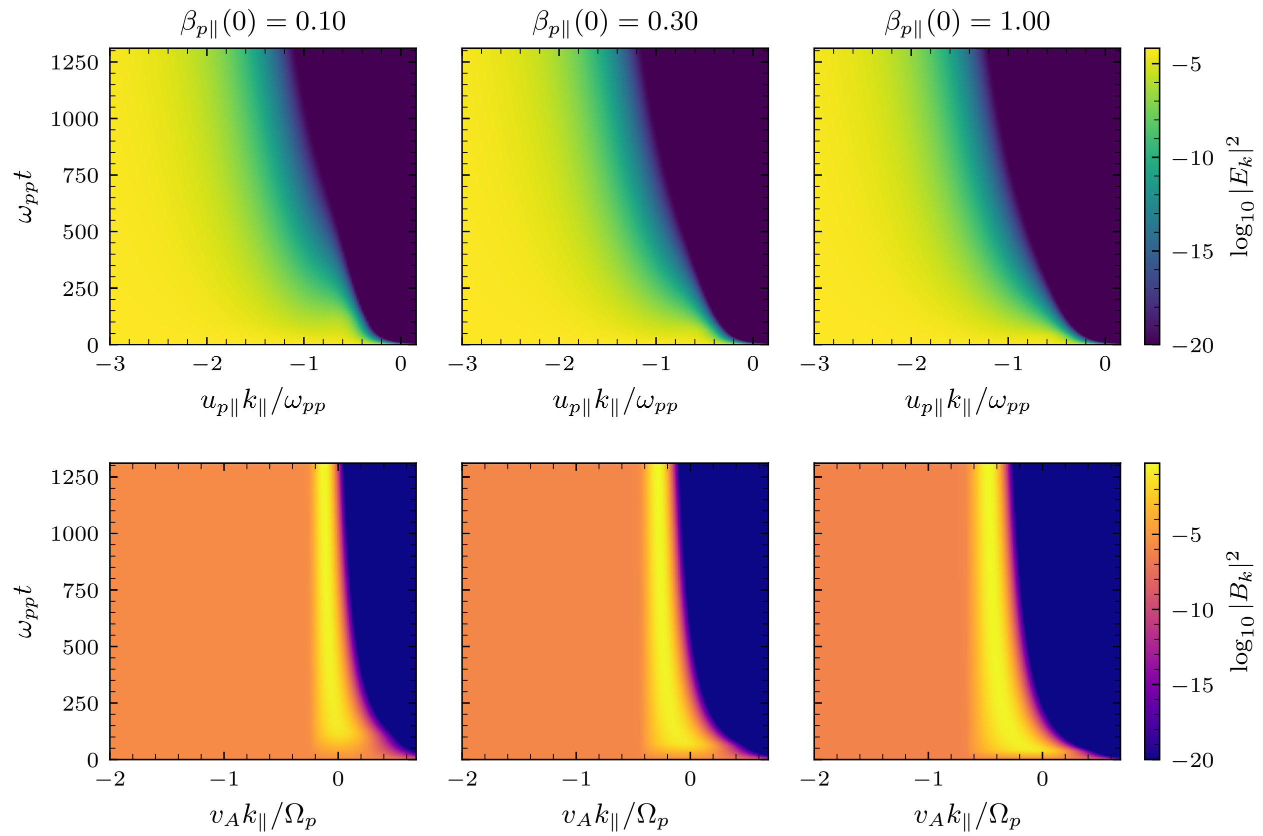

Figure 2.3.8: Time evolution of the electric (top row) and magnetic (bottom row) field power spectra as functions of their respective normalized wavenumbers, $u_p k_\parallel/\omega_{pp}$ and $v_A k_\parallel/\Omega_p$, shown on a logarithmic scale. Each column corresponds to a different initial proton parallel beta value $\beta_{p\parallel}$, as defined in Figure 2.3.7. All cases assume $|E_k|^2(0) = 10^{-4}$ for the electric field and $|B_k|^2(0) = 10^{-5}$ for the magnetic field. Color bar scale represents the logarithmic intensity of the fields over time.

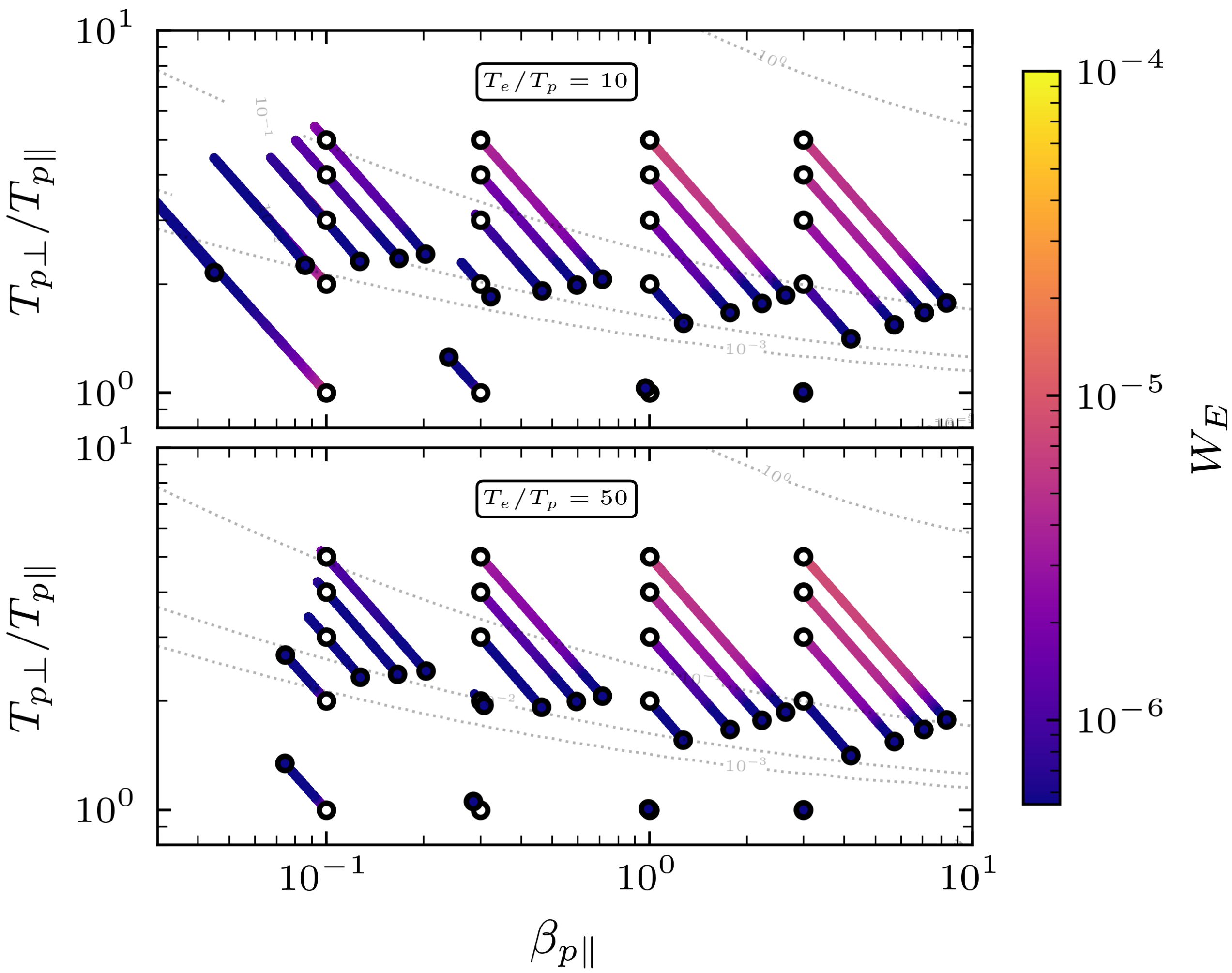

Figure 2.3.9: Quasilinear evolution of the proton $\beta_{p\parallel}$ and anisotropy $T_\perp/T_\parallel$ for two temperatures ratio, $T_e/T_p = 10$ (upper) and $T_e/T_p = 50$ (bottom). In both, initial conditions (white circles) were chosen evenly spaced in the range $0.1 \leq \beta_\parallel \leq 3$ and $1 \leq T_\perp/T_\parallel \leq 5$, with an uniform electric wave spectrum power of $W_E(0) = 10^{-4}$, an uniform magnetic wave spectrum power of $W_B(0) = 10^{-5}$ for all cases. The colorbar represent the instantaneous value of $W_E(t)$. Dashed lines are contours of the proton-cyclotron instability with maximum growth-rates $\gamma/\Omega_p = 10^{-3}$ to 10^0, as calculated from the dispersion relation Equation 2.2.2 considering the corresponding temperature ratio to $\beta_{e\parallel}$. Colorized circles correspond to the stationary (final) state of the plasma simulations.

Chapter 3

Discussion and Conclusions

In this work, we have employed quasilinear moment theory to investigate the effects of two initially independent wave spectra propagating parallel to a background magnetic field in a bi-Maxwellian proton plasma.

Our study primarily focused on understanding the role of wave-particle interactions in regulating proton temperature anisotropy, which is a common feature in weakly collisional space plasmas such as the solar wind. While linear theory predicts a decoupling between the electrostatic and electromagnetic spectra under the conditions considered, the results shown here demonstrate that the temperature ratio between electrons and protons plays a pivotal role in mediating their nonlinear coupling via electric field fluctuations, seeking to obtain an instability that competes with EMIC. More specifically, we have shown that even in the absence of initial correlations, the simultaneous presence of an electrostatic IAW and an electromagnetic ACW spectra results in a redistribution of energy that primarily affects the transverse proton temperature.

The modulation of this exchange depends sensitively on the value of T_e/T_p, confirming that electrons, despite not being directly involved in the ACW dynamics, act as mediators of energy flow through their contribution to electric field fluctuations. These findings suggest that quasilinear interactions between nominally independent wave modes can lead to emergent coupling mechanisms that regulate kinetic properties of protons, an effect not captured by linear dispersion theory alone.

We also note that efforts to couple, bridge, or mediate the scale separation between these two modes have been previously pursued using alternative numerical approaches and compared against spacecraft data. In particular, notable studies [13, 14] employed hybrid Vlasov-Maxwell and Vlasov-Yukawa simulations to address the orders-of-magnitude difference between Alfvén-Cyclotron scales and the Debye length. By introducing a *bump* in the distribution function, they identified a new type of ion-acoustic instability, termed the *ion-bulk* mode, which can survive Landau damping under near-isothermal conditions ($T_e \approx T_p$). These results were benchmarked against time intervals from the *STEREO* mission. However, such phenomena are not considered in this work, as our linear analysis shows that the specific IAW branch under consideration does not propagate under the studied conditions.

On the other hand, recent observational studies conducted closer to the Sun than ever before—between 13 and 25 solar radii—have identified the simultaneous presence of magnetosonic waves accompanied by acoustic-like dispersive modes that do not exhibit correlated magnetic fluctuations. These observations, which have also been compared with numerical simulations of both Vlasov and MHD type, have addressed possible resonance effects, albeit under oblique propagation with respect to the ambient magnetic field [60]. Furthermore, they report turbulent-like energy transfer and the absence of detectable daughter waves—features previously discussed in parametric numerical studies, which nonetheless have yet to pinpoint the origin of such fluctuations [17]. These findings highlight a potential avenue for extending the present work.

Today it is known that measurements from missions such as *WIND*, *ACE*, and *Helios* have shown that solar wind protons often exhibit anisotropic temperature distributions with $T_\perp/T_\parallel < 1$, particularly in high-speed streams [61]. Our results contribute to the theoretical understanding of how such anisotropies can be self-regulated by wave-particle interactions, and how the presence of different spectral components may either increase or suppress this interaction, depending on the background plasma parameters.

In the second part of our investigation, we focused on the influence of a fixed-amplitude electrostatic spectrum on a magnetized hydrogen plasma representative of solar wind conditions. This spectrum excites proton-acoustic instabilities that are sensitive to the ambient anisotropy. In contrast to previous studies that adopted cold or isothermal electron approximations [32, 37], we retained the full kinetic dynamics of both electrons and protons. This self-consistent treatment of electron thermal dynamics allowed for a more realistic assessment of the system's evolution and energy partition.

Importantly, we showed that most of the wave-induced heating is absorbed by protons, particularly in the perpendicular direction with respect to the magnetic field. This result reinforces the notion that transverse proton heating can be effectively driven by electrostatic fluctuations, especially in the presence of temperature anisotropy. Moreover, our use of a fixed Alfvén speed to light speed ratio $v_A/c = 0.1$, although artificially large, allowed us to explore the quasilinear dynamics over manageable computational timescales. This parameter effectively sets the timescale of the wave-particle interactions and influences the detuning between electrostatic and electromagnetic modes as seen in Figure 2.3.1 and Figure 2.3.2.

We have demonstrated that quasilinear moment theory provides a suitable and effective framework for studying weakly nonlinear wave-particle interactions in anisotropic, collisionless plasmas. In particular, our investigation highlights that:

1. Nominally independent wave spectra, such as electrostatic IAWs and electromagnetic ACWs, can interact indirectly via electron-to-proton temperature ratio along with electric field fluctuations, especially when $10 \leq T_e/T_p \leq 50$.

2. The presence of electrostatic spectra enhances transverse proton heating, thereby promoting the relaxation of temperature anisotropy.

3. Electrons, although not directly destabilized by the electromagnetic waves, mediate energy exchange processes and thus play an important role in the system's nonlinear evolution.

These findings support the idea that temperature anisotropies observed in the solar wind can be shaped not only by the direct resonant interactions typically accounted for in linear theory, but also by nonlinear couplings between multiple wave modes and species.

Our study complements and extends previous work on the quasilinear evolution of electromagnetic fluctuations [35, 36, 32, 37] by incorporating fully kinetic effects and a consistent treatment of electrostatic wave spectrum. By revealing how multiple spectral components influence the macroscopic plasma state, this work contributes to a more complete picture of energy dissipation and regulation in space plasmas.

While our model assumes a homogeneous and stationary background, as well as bi-Maxwellian velocity distributions, these simplifications were made to isolate the fundamental physics of quasilinear interactions. A natural next step involves extending the model to incorporate additional sources of free energy, such as drift velocities and a multi-species plasma composition, in order to test the robustness and generality of the mechanisms identified in this work. Possible improvements include time-evolving spectra, spectral slope breaks, non-Maxwellian distributions (e.g., kappa functions), and the use of expanding box models. The inclusion of minor-ion populations such as alpha particles or oxygen ions, due to their distinct inertia/mass-ratio contributions, could further enrich the analysis. Additionally, introducing relative drifts between species may allow for the study of current-driven instabilities, such as the Buneman or modified two-stream instability [62, 41, 63]. These extensions will be instrumental in advancing our understanding of particle energization, spectral energy transfer, and the constraints imposed on plasma anisotropies in the solar wind and related systems.

Bibliography

[1] P. H. Yoon, Reviews of Modern Plasma Physics **1**, 4 (2017).

[2] P. H. Yoon, R. A. López, J. Seough, M. Rashid, C. S. Salem, M. Sarfraz, M. Lazar, and S. M. Shaaban, The Astrophysical Journal **976**, 173 (2024).

[3] R. E. Navarro, J. Araneda, V. Muñoz, P. S. Moya, A. F-Viñas, and J. A. Valdivia, Physics of Plasmas **21**, 726 (2014).

[4] D. A. Gurnett and R. R. Anderson, Journal of Geophysical Research **82**, 632–650 (1977).

[5] S. P. Gary, Journal of Geophysical Research: Space Physics **83**, 2504–2510 (1978).

[6] F. Valentini, D. Perrone, F. Califano, F. Pegoraro, P. Veltri, P. J. Morrison, and T. M. O'Neil, Physics of Plasmas **19**, 092103 (2012).

[7] S. D. Bale, K. Goetz, P. R. Harvey, P. Turin, J. W. Bonnell, T. Dudok de Wit, R. E. Ergun, R. J. MacDowall, M. Pulupa, M. Andre, M. Bolton, J.-L. Bougeret, T. A. Bowen, D. Burgess, C. A. Cattell, B. D. G. Chandran, C. C. Chaston, C. H. K. Chen, M. K. Choi, J. E. Connerney, S. Cranmer, M. Diaz-Aguado, W. Donakowski, J. F. Drake, W. M. Farrell, P. Fergeau, J. Fermin, J. Fischer, N. Fox, D. Glaser, M. Goldstein, D. Gordon, E. Hanson, S. E. Harris, L. M. Hayes, J. J. Hinze, J. V. Hollweg, T. S. Horbury, R. A. Howard, V. Hoxie, G. Jannet, M. Karlsson, J. C. Kasper, P. J. Kellogg, M. Kien, J. A. Klimchuk, V. V. Krasnoselskikh, S. Krucker, J. J. Lynch, M. Maksimovic, D. M. Malaspina, S. Marker, P. Martin, J. Martinez-Oliveros, J. McCauley, D. J. McComas, T. McDonald, N. Meyer-Vernet, M. Moncuquet, S. J. Monson, F. S. Mozer, S. D. Murphy, J. Odom, R. Oliverson, J. Olson, E. N. Parker, D. Pankow, T. Phan, E. Quataert, T. Quinn, S. W. Ruplin, C. Salem, D. Seitz, D. A. Sheppard, A. Siy, K. Stevens, D. Summers, A. Szabo, M. Timofeeva, A. Vaivads, M. Velli, A. Yehle, D. Werthimer, and J. R. Wygant, Space Science Reviews **204**, 49 (2016).

[8] I. Alexeff, W. D. Jones, and D. Montgomery, Physical Review Letters **19**, 422–425 (1967).

[9] B. D. Fried, R. B. White, and T. K. Samec, Physics of Fluids **14**, 2388–2392 (1971).

[10] D. A. Gurnett, E. Marsch, W. Pilipp, R. Schwenn, and H. Rosenbauer, Journal of Geophysical Research: Space Physics **84**, 2029–2038 (1979).

[11] N. Krall and A. Trivelpiece, *Principle of Plasma Physics* (McGraw Hill Book Company, 1973) pp. 513 – 526.

[12] J. A. Araneda, E. Marsch, and A. F.-Viñas, Physical Review Letters **100**, 125003 (2008).

[13] F. Valentini, D. Perrone, and P. Veltri, The Astrophysical Journal **739**, 54 (2011).

[14] A. Vecchio, F. Valentini, S. Donato, V. Carbone, C. Briand, J. Bougeret, and P. Veltri, Journal of Geophysical Research: Space Physics **119**, 7012–7024 (2014).

[15] D. Verscharen, K. G. Klein, and B. A. Maruca, Living Reviews in Solar Physics **16**, 5 (2019), 136 pp.

[16] J. L. Verniero, D. E. Larson, R. Livi, A. Rahmati, M. D. McManus, P. S. Pyakurel, K. G. Klein, T. A. Bowen, J. W. Bonnell, B. L. Alterman, P. L. Whittlesey, D. M. Malaspina, S. D. Bale, J. C. Kasper, A. W. Case, K. Goetz, P. R. Harvey, K. E. Korreck, R. J. MacDowall, M. Pulupa, M. L. Stevens, and T. D. de Wit, The Astrophysical Journal Supplement Series **248**, 5 (2020).

[17] P. J. Kellog, F. S. Mozer, M. Moncuquet, D. M. Malaspina, J. Halekas, S. D. Bale, and K. Goetz, The Astrophysical Journal **964**, 68 (2024).

[18] F. Valentini, P. Trávníček, F. Califano, P. Hellinger, and A. Mangeney, Journal of Computational Physics **225**, 753–770 (2007).

[19] F. Valentini, F. Califano, D. Perrone, F. Pegoraro, and P. Veltri, Physical Review Letters **106**, 165002 (2011).

[20] A. A. Vlasov, Soviet Physics Uspekhi **10**, 721–733 (1968).

[21] Y. L. Klimontovich, *Statistical Theory of Open Systems* (Springer Netherlands, 1995) p. 117–129.

[22] S. Ichimaru, *Basic Principles of Plasma Physics* (CRC Press, 1973) pp. 295 – 301.

[23] R. K. Pathria and P. D. Beale, *Statistical Mechanics* (Elsevier, 2011) pp. 25 – 29.

[24] N. Rostoker and M. N. Rosenbluth, Physics of Fluids **3**, 1 (1960).

[25] N. N. Bogoliubov, Journal of Experimental and Theoretical Physics USSR **10**, 265 (1946).

[26] R. C. Davidson, Journal of Plasma Physics **12**, 151 (1972).

[27] D. G. Swanson, *Plasma Waves*, 2nd ed. (Institute of Physics Publishing, 2003) pp. 334 – 346.

[28] S. Peter Gary, *Theory of Space Plasmas Microinstabilities* (Cambridge University Press, 1993) pp. 31, 100.

[29] E. Marsch, Nonlinear Processes in Geophysics **5**, 111 (1998).

[30] F. Valentini and P. Veltri, Physical Review Letters **102**, 225001 (2009).

[31] J. A. Araneda, H. F. Astudillo, and E. Marsch, Space Science Reviews **172**, 361–372 (2011).

[32] P. S. Moya and R. E. Navarro, Frontiers in Physics **9**, 1 (2021).

[33] F. Valentini, A. Vecchio, S. Donato, V. Carbone, C. Briand, J. Bourgeret, and P. Veltri, The Astrophysical Journal **788**, 1 (2014).

[34] F. S. Mozer, S. D. Bale, C. A. Cattell, J. Halekas, I. Y. Vasko, J. L. Verniero, and P. J. Kellogg, The Astrophysical Journal Letters **927**, L15 (2022).

[35] M. Lazar, P. H. Yoon, R. A. López, and P. S. Moya, Journal of Geophysical Research: Space Physics **123**, 6–19 (2018).

[36] S. M. Shaaban, M. Lazar, P. H. Yoon, and S. Poedts, Astronomy & Astrophysics **627**, A76 (2019).

[37] R. E. Navarro and P. S. Moya, Universe **9**, 12 (2023).

[38] T. O'Neil, Physics of Fluids **8**, 2255 (1965).

[39] C. Y. Tu and E. Marsch, Space Science Reviews **73**, 1 (1995).

[40] D. E. Muller, Mathematical Tables and Other Aids to Computation **10**, 208 (1956).

[41] T. J. M. Boyd and J. J. Sanderson, *The Physics of Plasmas* (Cambridge University Press, 2003) pp. 265 – 272, 274.

[42] R. W. Fredricks and C. F. Kennel, Journal of Geophysical Research **73**, 7429–7435 (1968).

[43] S. P. Gary, Journal of Plasma Physics **35**, 431–447 (1986).

[44] K. Liu, S. P. Gary, and D. Winske, Journal of Geophysical Research: Space Physics **116**, A07212 (2011), 12 pp.

[45] M. Porkolab, in *American Institute of Physics Conference Proceedings*, Vol. 314 (American Institute of Physics, 1994) p. 99–127.

[46] M. Brambilla, Plasma Physics and Controlled Fusion **41**, 1–34 (1999).

[47] V. Duarte, H. Berk, N. Gorelenkov, W. Heidbrink, G. Kramer, R. Nazikian, D. Pace, M. Podestà, B. Tobias, and M. Van Zeeland, Nuclear Fusion **57**, 054001 (2017).

[48] H. Alfvén, Nature **150**, 405–406 (1942).

[49] S. P. Gary and J. E. Borovsky, Journal of Geophysical Research: Space Physics **109**, A06105 (2004), 12 pp.

[50] G. G. Howes, W. Dorland, S. C. Cowley, G. W. Hammett, E. Quataert, A. A. Schekochihin, and T. Tatsuno, Physical Review Letters **100**, 065004 (2008).

[51] J. C. Kasper, A. J. Lazarus, and S. P. Gary, Physical Review Letters **101**, 261103 (2008).

[52] L. Gomberoff, V. Muñoz, and J. Valdivia, Planetary and Space Science **52**, 679–684 (2004).

[53] P. S. Moya, A. F. Viñas, V. Muñoz, and J. A. Valdivia, Annales Geophysicae **30**, 1361–1369 (2012).

[54] R. E. Navarro, V. Muñoz, J. A. Valdivia, and P. S. Moya, The Astrophysical Journal Letters **898**, L9 (2020).

[55] P. A. Isenberg, M. A. Lee, and J. V. Hollweg, Journal of Geophysical Research: Space Physics **106**, 5649–5660 (2001).

[56] D. Píša, J. Souček, O. Santolík, M. Hanzelka, G. Nicolaou, M. Maksimovic, S. D. Bale, T. Chust, Y. Khotyaintsev, V. Krasnoselskikh, M. Kretzschmar, E. Lorfèvre, D. Plettemeier, M. Steller, v. Štverák, P. Trávníček, A. Vaivads, A. Vecchio, T. Horbury, H. O'Brien, V. Evans, V. Angelini, C. J. Owen, and P. Louarn, Astronomy & Astrophysics **656**, A14 (2021).

[57] V. K. Yadav, IETE Technical Review **37**, 3–11 (2018).

[58] N. J. Fox, M. C. Velli, S. D. Bale, R. Decker, A. Driesman, R. A. Howard, J. C. Kasper, J. Kinnison, M. Kusterer, D. Lario, M. K. Lockwood, D. J. McComas, N. E. Raouafi, and A. Szabo, Space Science Reviews **204**, 7–48 (2015).

[59] S. D. Bale, S. T. Badman, J. W. Bonnell, T. A. Bowen, D. Burgess, A. W. Case, C. A. Cattell, B. D. G. Chandran, C. C. Chaston, C. H. K. Chen, J. F. Drake, T. D. de Wit, J. P. Eastwood, R. E. Ergun, W. M. Farrell, C. Fong, K. Goetz, M. Goldstein, K. A. Goodrich, P. R. Harvey, T. S. Horbury, G. G. Howes, J. C. Kasper, P. J. Kellogg, J. A. Klimchuk, K. E. Korreck, V. V. Krasnoselskikh, S. Krucker, R. Laker, D. E. Larson, R. J. MacDowall,

M. Maksimovic, D. M. Malaspina, J. Martinez-Oliveros, D. J. McComas, N. Meyer-Vernet, M. Moncuquet, F. S. Mozer, T. D. Phan, M. Pulupa, N. E. Raouafi, C. Salem, D. Stansby, M. Stevens, A. Szabo, M. Velli, T. Woolley, and J. R. Wygant, Nature **576**, 237–242 (2019).

[60] I. Y. Vasko, F. S. Mozer, T. Bowen, J. Verniero, X. An, A. V. Artemyev, S. D. Bale, J. W. Bonnell, J. Halekas, and I. V. Kuzichev, The Astrophysical Journal Letters **967**, L31 (2024).

[61] S. D. Bale, J. C. Kasper, G. G. Howes, E. Quataert, C. Salem, and D. Sundkvist, Physical Review Letters **103**, 211101 (2009).

[62] O. Buneman, Physical Review **115**, 503–517 (1959).

[63] P. H. Yoon and T. Umeda, Physics of Plasmas **17**, 112317 (2010).

Appendix A

A1 Moment calculations

$$\int dv_\perp dv_\| \frac{v_\perp}{\omega_k - v_\| k}\frac{\partial F_\mu}{\partial v_\|} = \frac{1}{\omega_k}\int dv_\perp dv_\| \frac{v_\perp}{\omega_k - v_\| k}\left[1+\frac{v_\| k}{\omega_k - v_\| k}\right]\frac{\partial F_\mu}{\partial v_\|}, \tag{A1.1}$$

$$= \frac{k}{\omega_k}\int dv_\perp dv_\| \frac{v_\perp v\,\|}{\omega_k - v_\| k}\frac{\partial F_\mu}{\partial v_\|}, \tag{A1.2}$$

$$= \frac{2k}{\omega_{p\mu}^2}\chi_\mu^{zz}. \tag{A1.3}$$

A2 Susceptibilities with a bi-Maxwellian distribution

A2.1 Transverse susceptibility

For this calculation we will define $t = v_\|/u_{\|\mu}$, $R_\mu = u_{\perp\mu}^2/u_{\|\mu}^2$ and $A_\mu = R_\mu - 1$.

$$\begin{aligned}
\chi_\mu^{(\pm)} &= \frac{\omega_{p\mu}^2}{4\omega^2}\int dv_\perp dv_\| \frac{v_\perp^2}{\omega - v_\| k \pm \Omega_\mu}\left[(\omega - \boldsymbol{v}\cdot\boldsymbol{k})\frac{\partial F_\mu}{\partial v_\perp} + v_\perp k\frac{\partial F_\mu}{\partial v_\|}\right],\\
&= \frac{\omega_{p\mu}^2}{2\omega^2}\frac{1}{\pi^{3/2}u_{\perp\mu}^4 u_{\|\mu}}\underbrace{\int_0^\infty dv_\perp v_\perp^3 \exp\left[-\frac{v_\perp^2}{u_{\perp\mu}^2}\right]}_{u_{\perp\mu}\sqrt{\pi}/2}\int_{-\infty}^\infty dv_\| \frac{\omega + (R_\mu - 1)v_{\|k}}{v_\| k - \omega \mp \Omega_\mu}\exp\left[-\frac{v_\|^2}{u_{\|\mu}^2}\right],\\
&= \frac{\omega_{p\mu}^2}{4\omega^2}\frac{1}{\pi^{3/2}u_{\|\mu}}\int_{-\infty}^\infty dv_\| \left[(R_\mu - 1) + \frac{\omega - (R_\mu - 1)(\omega \pm \Omega_\mu)}{v_\| k - (\omega \pm \Omega_\mu)}\right]\exp\left[-\frac{v_\|^2}{u_{\|\mu}^2}\right], \qquad \text{(A2.1)}\\
&= \frac{\omega_{p\mu}^2}{4\omega^2}\frac{1}{\pi^{3/2}}\int_{-\infty}^\infty dt\left[(R_\mu - 1) + \frac{\xi_\mu^0 + (R_\mu - 1)\xi_\mu^\pm}{t - \xi_\mu^\pm}\right]e^{-t^2},\\
&= \frac{\omega_{p\mu}^2}{4\omega^2}\frac{1}{\pi^{3/2}}\left\{(R_\mu - 1) + [\xi_\mu^0 + (R_\mu - 1)\xi_\mu^\pm]Z(\xi_\mu^\pm)\right\},\\
&= \frac{\omega_{p\mu}^2}{4\pi\omega^2}[A_\mu + (\xi_\mu^0 + A_\mu\xi_\mu^\pm)Z(\xi_\mu^\pm)].
\end{aligned}$$

Thus, the electromagnetic dispersion for transverse waves

$$\begin{aligned} 1-\frac{c^2k^2}{\omega^2}+4\pi\sum_\mu \chi_\mu^{(\pm)}=0, \\ 1-\frac{c^2k^2}{\omega^2}+\sum_\mu \frac{\omega_{p\mu}^2}{\omega^2}[A_\mu+(\xi_\mu^0+A_\mu\xi_\mu^\pm)Z(\xi_\mu^\pm)]=0. \end{aligned} \tag{A2.2}$$

A2.2 Longitudinal susceptibility

We will define $t=v_\parallel/u_{\parallel\mu}$ and $\xi_\mu=\omega/u_{\parallel\mu}k$.

$$\begin{aligned}
\chi_\mu^{zz} &= \frac{\omega_{p\mu}^2}{2\omega}\int dv_\perp dv_\parallel \frac{v_\perp v_\parallel}{\omega - v_{\parallel k}}\frac{\partial F_\mu}{\partial v_\parallel}, \\
&= \frac{\omega_{p\mu}^2}{2\omega}\frac{1}{\pi^{3/2}u_{\perp\mu}^2 u_{\parallel\mu}^3}\int dv_\perp dv_\parallel \frac{v_\perp v_\parallel^2}{v_\parallel k-\omega}\exp\left[-\frac{v_\perp^2}{u_{\perp\mu}^2}-\frac{v_\parallel^2}{u_{\parallel\mu}^2}\right], \\
&= \frac{\omega_{p\mu}^2}{\omega k}\frac{1}{\pi^{3/2}u_{\perp\mu}^2 u_{\parallel\mu}^3}\underbrace{\int_0^\infty dv_\perp v_\perp \exp\left[-\frac{v_\perp^2}{u_{\perp\mu}^2}\right]}_{u_{\perp\mu}^2/2}\int_{-\infty}^\infty dv_\parallel \frac{v_\parallel^2}{v_\parallel-\omega/k}\exp\left[-\frac{v_\parallel^2}{u_{\parallel\mu}^2}\right], \\
&= \frac{\omega_{p\mu}^2}{\omega k}\frac{1}{2\pi^{3/2}u_{\parallel\mu}^3}\int_{-\infty}^\infty dv_\parallel \frac{v_\parallel^2}{v_\parallel-\omega/k}\exp\left[-\frac{v_\parallel^2}{u_{\parallel\mu}^2}\right], \\
&= \frac{\omega_{p\mu}^2}{\omega k}\frac{1}{2\pi^{3/2}u_{\parallel\mu}^3}\int_{-\infty}^\infty dv_\parallel \left[v_\parallel^2+\frac{\omega}{k}\left(1+\frac{\omega/k}{v_\parallel-\omega/k}\right)\right]\exp\left[-\frac{v_\parallel^2}{u_{\parallel\mu}^2}\right], \\
&= \frac{\omega_{p\mu}^2}{\omega k}\frac{1}{2\pi^{3/2}u_{\parallel\mu}}\int_{-\infty}^\infty dt\left[t+\frac{\omega}{u_{\parallel\mu}k}\left(1+\frac{\xi_\mu}{t-\xi_\mu}\right)\right]e^{-t^2}, \\
&= \frac{\omega_{p\mu}^2}{u_{\parallel\mu}^2 k^2}\frac{1}{2\pi}[1+\xi_\mu Z(\xi_\mu)].
\end{aligned} \tag{A2.3}$$

Let us notice that the sum over all the domain for te^{-t^2} is null since it is an odd function. Also, we have used $Z(\xi)$ the plasma dispersion function defined as

$$Z(\xi)=\frac{1}{\sqrt{\pi}}\int_{-\infty}^\infty dt\frac{e^{-t^2}}{t-\xi}. \tag{A2.4}$$

A3 Electromagnetic dispersion relation (cold electrons approximation)

We will work the electromagnetic dispersion relation for a plasma compound by protons and electrons with left-handed polarization.

$$
\begin{aligned}
1-\frac{c^2k^2}{\omega^2}+\sum_{\mu}\frac{\omega_{p\mu}^2}{\omega^2}[A_\mu+(\xi_\mu^0+A\xi^-)Z(\xi_\mu^-)]&=0,\\
1-\frac{c^2k^2}{\omega^2}+\frac{\omega_{pp}^2}{\omega^2}[A_p+(\xi_p^0+A\xi^-)Z(\xi_p^-)]+\frac{\omega_{pe}^2}{\omega^2}[A_e+(\xi_e^0+A\xi^-)Z(\xi_e^-)]&=0,\\
\frac{\omega^2}{\omega_{pp}^2}-\frac{c^2k^2}{\omega_{pp}^2}+[A_p+(\xi_p^0+A\xi_p^-)Z(\xi_p^-)]+\frac{\omega_{pe}^2}{\omega_{pp}^2}[A_e+(\xi_e^0+A\xi^-)Z(\xi_e^-)]&=0.
\end{aligned}
\tag{A3.1}
$$

It is defined $\omega^2/\omega_{pp}^2=\omega^2v_A^2/\Omega_p^2c^2$ and $c^2k^2/\omega_{pp}^2=v_A^2k^2/\Omega_p^2$. Then, using the hot electrons approximation ($\xi_e<1$) at first order, meaning $Z(\xi_e^-)\approx-2\xi_e^-$, and by making $n_e/n_p=1$ accomplishing quasineutrality, we write again

$$
\begin{aligned}
\frac{\omega^2}{\Omega_p^2}\frac{v_A^2}{c^2}-\frac{v_A^2k^2}{\Omega_p^2}+[A_p+(\xi_p^0+A\xi^-)Z(\xi_p^-)]+\frac{n_e}{n_p}[A_e+(\xi_e^0+A\xi_e^-)\cdot(-2\xi_e^-)]&=0,\\
\frac{\omega^2}{\Omega_p^2}\frac{v_A^2}{c^2}-\frac{v_A^2k^2}{\Omega_p^2}+[A_p+(\xi_p^0+A\xi^-)Z(\xi_p^-)]+[A_e+(\xi_e^0+A\xi_e^-)\cdot(-2\xi_e^-)]&=0.
\end{aligned}
\tag{A3.2}
$$

Let us briefly analyse the electron term, where it is clear that we get a second order term in the resonance ξ_e^-. Yet, the other term is not trivial.

$$
\xi_e^0\cdot\xi_e^-=\frac{\omega(\omega-\Omega_e)}{u_{\parallel e}^2k^2}=\frac{\omega^2}{u_{\parallel e}^2k^2}-\frac{\omega\Omega_e}{u_{\parallel e}^2k^2}.
\tag{A3.3}
$$

Then again, $\omega^2/u_{\parallel e}^2k^2$ is a second order term, thus it is too fast, so null. On the other hand, $|\Omega_e|\gg\omega$ hence, we can also neglect it.

Therefore,

$$
\frac{\omega^2}{\Omega_p^2}\frac{v_A^2}{c^2}-\frac{v_A^2k^2}{\Omega_p^2}+[A_p+(\xi_p^0+A\xi^-)Z(\xi_p^-)]+A_e=0.
\tag{A3.4}
$$

Let us notice that under this hot electrons approximation an electron anisotropy term is relevant. Nonetheless, we will consider them isotropic thus also null due $A_\mu=R_\mu-1$. By this point, we have obtained the transverse electromagnetic mode for kinetic protons that is employed in [32]. We have chosen electrons to not contribute explicitly to the plasma dynamics.